

## CHAPTER 2

### EXPERIMENTAL RIG DESCRIPTION

Two rotor set-ups were used to evaluate the effectiveness of an AMD to reduce nonsynchronous vibrations. Initially, experiments were conducted in a single-disk (three-mass total with two masses representing the AMB rotors) flexible rotor and then further tests were carried out in a three-disk (five-mass including the radial rotors of the AMBs) rotor simulating more properly the dynamics of a turbomachine. The rotors are supported in conventional bearings and two AMB are placed in each rotor, one is used as a source of excitation while the other provides active control. A detailed description of each of these set-ups is presented in the following sections.

#### 2.1 Test Rotors

##### 2.1.1 Single-Disk Rotor

Figure 2.1 shows the schematic for the single-disk experimental apparatus.

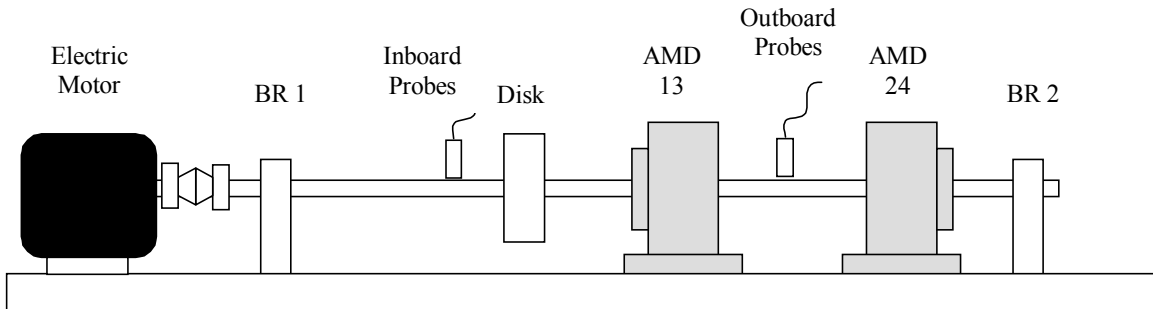


Figure 2.1: Schematic showing the single-disk rotor kit configuration (not to scale)

This rotor was assembled using a 9.52 mm (0.375 inch) steel shaft and one mass, a steel disk 72.2 mm (3 in) diameter, 25.4 mm (1 in) thick and a weight of 657 gr. (1.45 lbs), placed at approximately one third of the rotor span, 180.98 mm (7.125 in) from the coupling. The rotor was supported in two bronze sleeve bearings with a bearing span of

355.6 mm (14.0 in). The rotor had a total length of 457.2 mm (18.0 inches) and weighs 1.7 kg (3.78 lb).

Two radial rotors representing the rotating part of the AMDs, 34.3 mm (1.35 in) in diameter, 47.8 mm (1.88 in) long and a weight of 264 gr. (0.58 lbs) each, were attached to the shaft at approximately the midspan, 232.4 mm (9.150 in) from the coupling, and at three quarters of the rotor span, 342.9 mm (13.500 in) from the coupling respectively. The AMD placed at the midspan will be referred as AMD-13, and the AMD located at the outboard will be referred as AMD-24. Figure 2.2 shows the single-mass rotor kit.

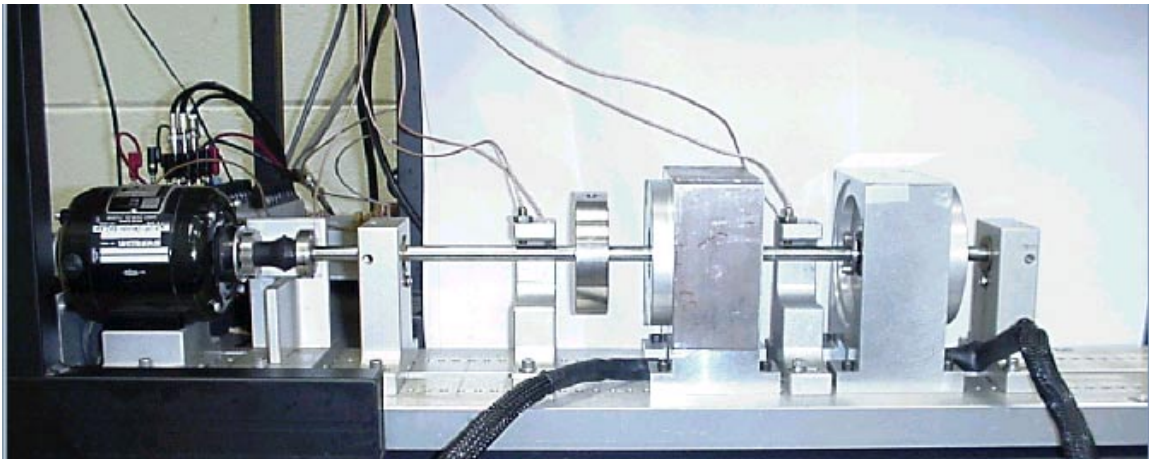


Figure 2.2: Single-disk rotor kit

### **2.1.2 Three-Disk Rotor**

The three-disk rotor was assembled using a steel shaft 9.52 mm (0.375 inch) in diameter and 641.4 mm (25.25 in) long, one steel disk 72.2 mm (3 in) diameter, 25.4 mm (1 in) thick and a weight of 657 gr. (1.45 lbs) placed at the midspan, 285.8 mm (11.25 in) from the coupling and two steel disks 72.2 mm (3 in) diameter, 19.1 mm (0.75 in) thick and a weight of 493 gr. (1.08 lb) each placed together close to the outboard end of the shaft, 600 mm (23.63 in) from the coupling. The rotor was supported in two bronze sleeve bearings with a bearing span of 463.6 mm (18.25 in) and weighs 3.95 kg (8.71 lb). Figure 2.3 shows the schematic of the three-disk experimental apparatus.

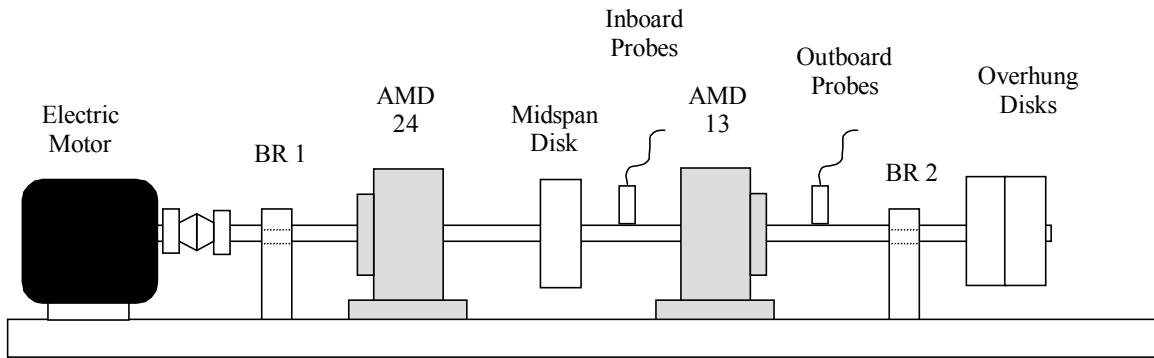


Figure 2.3: Schematic showing the three-disk rotor kit configuration (not to scale)

The AMB-24 was placed at approximately one quarter of the rotor span and its radial rotor was attached to the shaft at 155.5 mm (6.1 in) from the coupling. The AMB-13 was located at two thirds of the rotor span and its radial rotor was attached to the shaft at 406.4 mm (16.0 in) from the coupling. Both radial rotors are 34.3 mm (1.35 in) in diameter, 47.8 mm (1.88 in) long and with a weight of 264 gr. (0.58 lbs). Figure 2.4 shows the three-mass rotor kit.

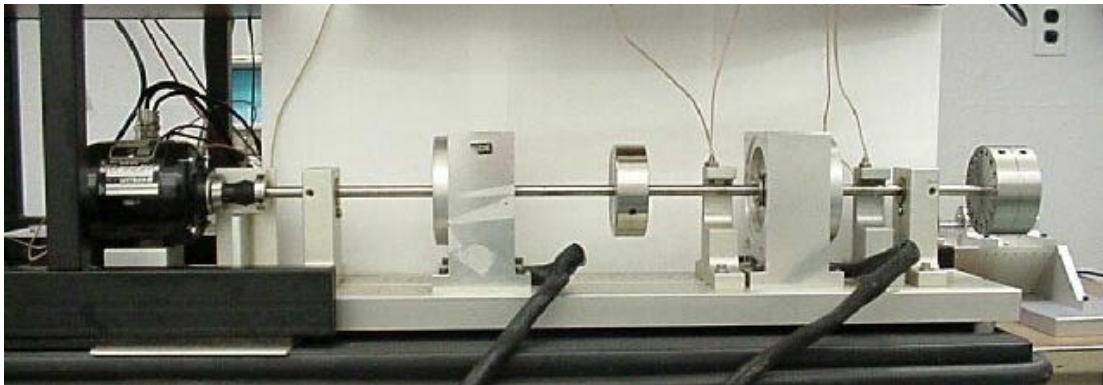


Figure 2.4: Three-disk rotor kit

Both rotor assemblies were attached to a steel base with a length of 787 mm (31.0 in), a width of 152 mm (6.0 in) and a thickness of 25 mm (1.0 in) and driven by a 0.1hp electric motor rated up to 10,000 RPM. A flexible coupling connected the rotors to the electric motor

## **2.2 Instrumentation**

A total of six proximity probes were used in each rotor. One was used as a speed sensor, connected to the motor speed controller, another one as key-phasor and the other four distributed in two sets or planes, one horizontal (X) and one vertical (Y) for each plane, to monitor shaft displacements. The first set identified as the inboard probes and the second set labeled as outboard probes. For the single-disk rotor, the inboard probes are located at 136.5 mm (5.375 in) from the coupling and the outboard probes are located at 298.5 mm (11.75 in) from the same reference. For the three-disk rotor, the inboard probes were located at 374.7 mm (14.75 in) and the outboard probes at 501.7 mm (19.75 in), both references from the coupling.

The inboard and outboard probes, as well as the key-phasor, were connected to a Bently Nevada Rotor Kit Proximitors Assembly and from there, the signals were taken to an interface and then to a Bently Nevada Data Acquisition Interface Unit (DAIU). The Bently Nevada Automated Diagnostics for Rotating Equipment software (ADRE for Windows) used on a Gateway Pentium III computer displayed and recorded the data collected from the two planes of probes.

## **2.3 Magnetic Bearing Rotor Research Test Stand**

The equipment used to excite the test rotors and to apply active control, consists of two radial AMBs, a MB350 controller, the MB Scope software and a MB Research Box manufactured by Revolve Magnetic Bearings Inc.

### **2.3.1 Radial AMBs**

Two radial AMBs were used in the experimental rig, each one consists of a radial rotor, a stator, a position sensor ring and a backup bearing. The radial rotor and the stator are used to levitate the rotor while the sensor ring measures radial position of the shaft for feedback. The backup bearing provides support to the rotor when the bearing is turned off or in case of a power loss. The AMBs characteristics are listed in Table 2.1 and their parts are shown in Figure 2.5. Each Radial AMB has two axes of control. Figure 2.6 shows the orientation of these axes.

Table 2.1: Radial magnetic bearing specifications

<b>Bearing Performance Specifications</b>	<b>Metric Units</b>	<b>Imperial Units</b>
Static load capacity	53 N	12 lbf
Saturation current	3.00 A	
Number of poles per quadrant	2	
Stator stack length	12.700 mm	0.500 in
Stator OD	70.822 mm	2.788 in
Stator ID	35.052 mm	1.380 in
Rotor OD	34.290 mm	1.350 in
Rotor lamination ID	23.275 mm	0.916 in
Nominal gap	0.381 mm	0.015 in
Small pole width	5.245 mm	0.207 in
Pole height	12.587 mm	0.496 in
Slot width (at ID)	8.417 mm	0.331 in
Pole centerline angle	0.394 rads	22.5 deg



Figure 2.5: Radial magnetic bearing disassembled showing the radial rotor the stator and the back-up bearing

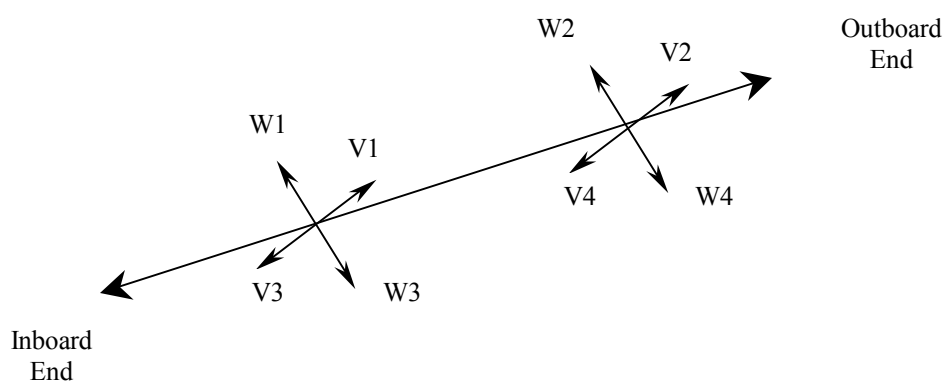


Figure 2.6: AMBs axes orientation

### 2.3.2 MB350 Controller

The MB350 is a Proportional-Integral-Derivative (PID) digital control system with a sampling frequency of 10000 Hz that offers five axis of magnetic bearing control, two axes per Radial AMB and one axis for a thrust AMB (not used in this research). The AMBs were connected to the MB350 controller through a machine connector. The controller, which has built-in amplifiers, takes signals from the sensors and computes the necessary stabilizing current requested to keep the rotor in the desired position.

### 2.3.3 MB Scope Software and MB Research

MB Scope is a computer program that allows monitoring internal system information and is required to perform parameter adjustment of the radial magnetic bearings. Table 2.2 lists the parameter tuning values used in this research. MB Scope Software was loaded on an IBM Pentium computer and connected to the MB350 controller through a parallel port connector. This system is also used for signal injection through the MB Research Box, which is a BNC connector based input/output box. Five axes (channels) of injection are available, four radial axes, V13, W13, V24 and W24, and one axial axis (Z2). The MB Research was connected to the MB 350 Controller at the diagnostic port.

Table 2.2: AMBs parameter tuning values

<b>Parameter</b>	<b>Value</b>
Max.current	2.0
Integral Gain	100.0
Proportional Gain	90
Derivative Gain	0.2
Total Gain	0.00008
Low pass 1	1500
LP damping 1	0.707
Top Bias current	0.75
Bottom Bias current	0.75

## 2.4 Undamped Critical Speed Analysis

An undamped critical speed analysis was performed using VT Fast, Virginia Tech Rotordynamic Laboratory code, on the single-disk rotor and the three-disk rotor. The results are presented below.

### 2.4.1 Single-Disk Rotor Critical Speeds

Three different configurations were considered for the single-disk rotor. The first one corresponded to the rotor supported on its conventional bearings and the AMDs off as shown in Figure 2.7. In order to study the effect that turning the AMDs on would have on the dynamics of the rotor, two more configurations were analyzed, one considering the AMD-13 (midspan) as a third bearing or damper, shown in Figure 2.8, and another one considering the AMD-24 (outboard) as a third bearing or damper, shown in Figure 2.9.

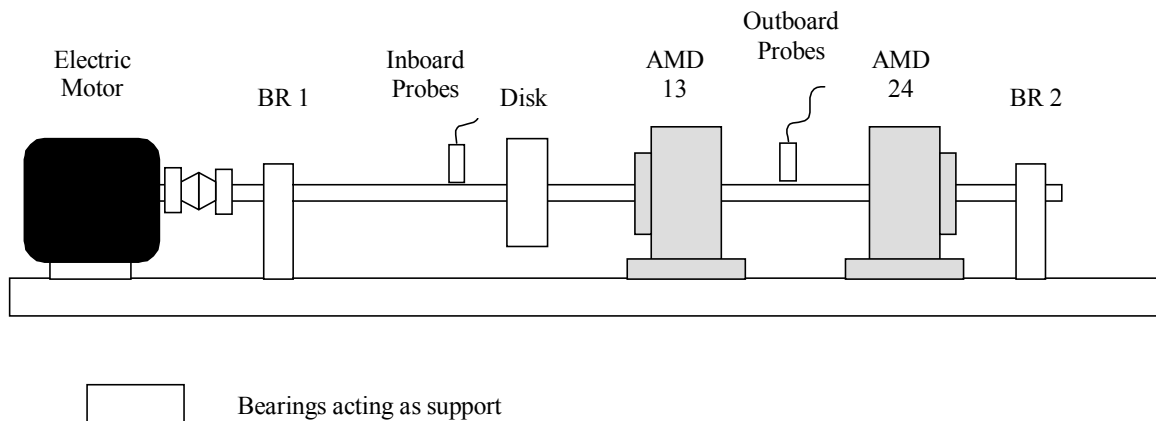


Figure 2.7: Schematic showing the single-disk rotor supported on its conventional bearings (not to scale)



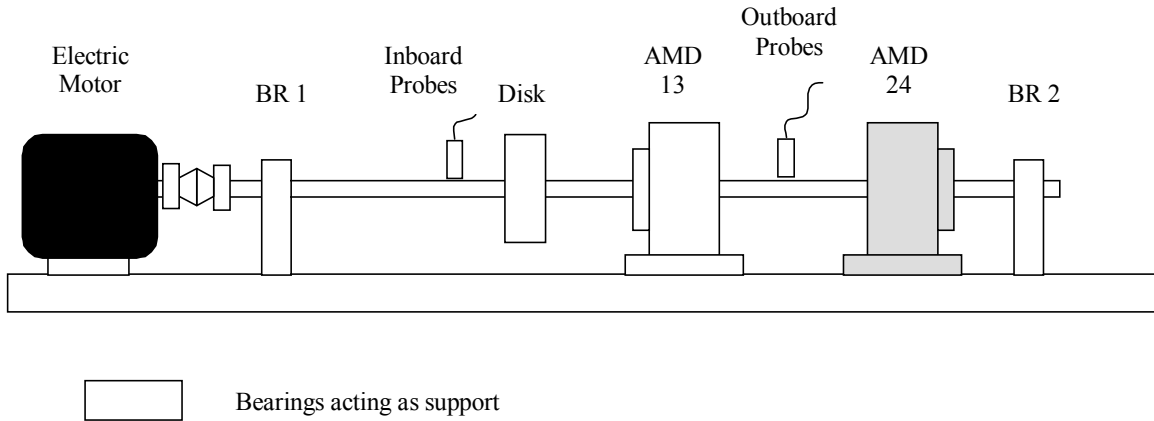


Figure 2.8: Schematic showing the single-disk rotor supported on its conventional bearings and the AMD-13 (not to scale)

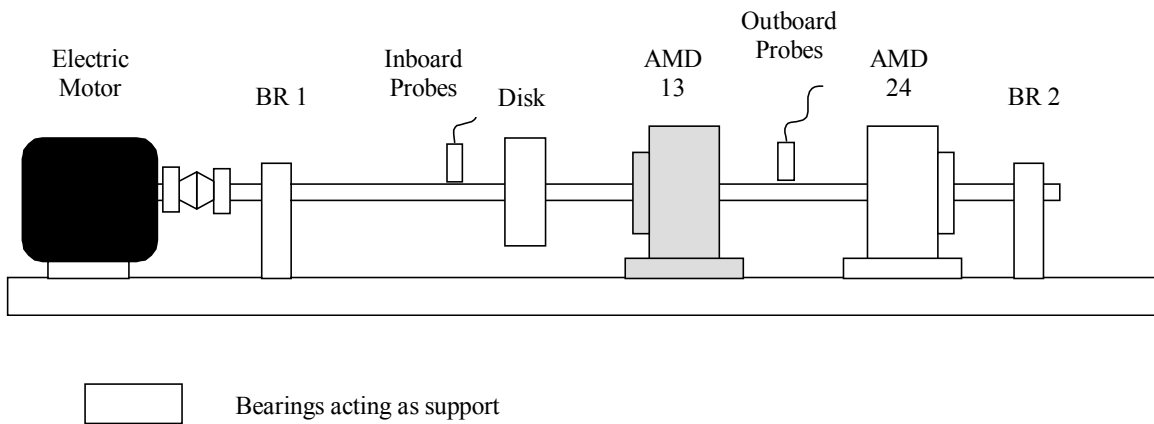


Figure 2.9: Schematic showing the single-disk rotor supported on its conventional bearings and the AMD-24 (not to scale)

### 2.4.1.1 Rotor with AMDs off

The model of the single-disk rotor with the AMDs off is listed in Table 2.3 and Figure 2.10 shows its graphic representation. This model was used as input file in the undamped critical speed program (CRTSPD) of the Virginia Tech Rotordynamics Laboratory VT Fast program. The stiffness (788 lbf/in) and damping (8 lbf-s/in) of the bronze support bearings, previously calculated by students of the Virginia Tech Rotordynamic Laboratory (Kirk, 1997) were initially used in this analysis resulting in a calculated undamped first critical speed of 2575 RPM (42.9 Hz). This value was 22.7% below the measured damped critical speed, 3160 RPM (52.7 Hz). The fluid film support bearing stiffness was then approximated as 1800 lb/in, based on a comparison to experimental run-up data to determine the actual location of rotor critical speeds. The Bode plot obtained experimentally using ADRE is shown in Figure 2.11. Figure 2.12 shows the undamped critical speed map. The calculated undamped first critical speed is 2918 RPM (48.6 Hz), this value is within 8.3% of the measured damped critical speed, 3160 RPM (52.7 Hz). Figure 2.13 shows the mode shapes for this configuration. The second critical speed is not discussed in this analysis because is not in the operational range of the rotor kit.

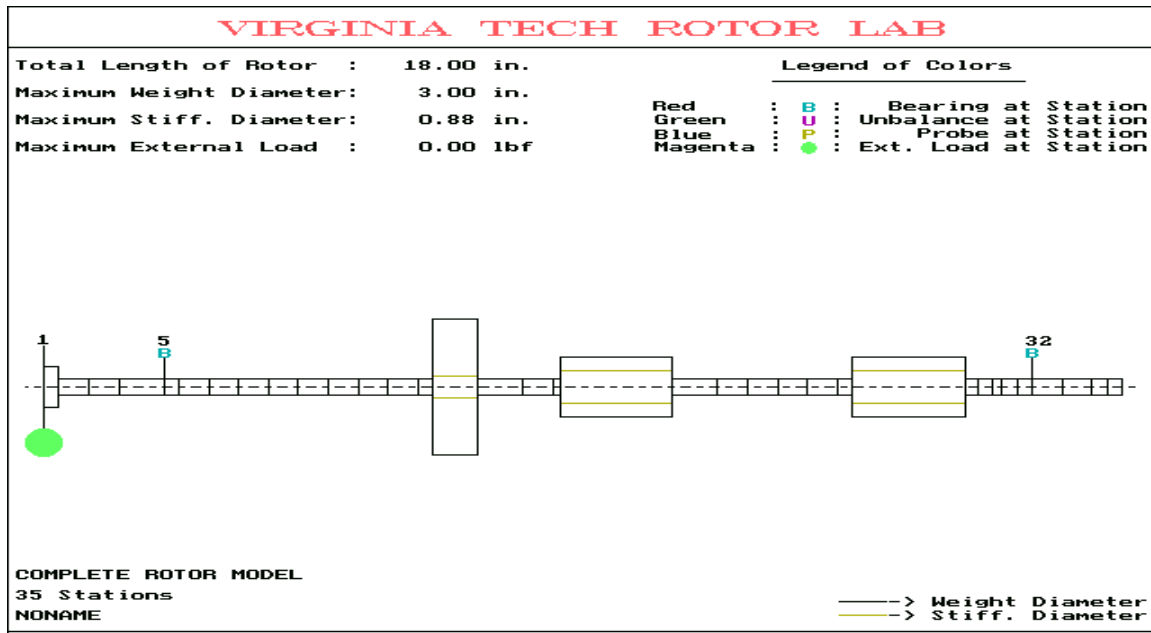


Figure 2.10: VT Fast graphic representation of the single-disk rotor supported on its conventional bearings with the AMDs off.  $K_{FFB}=1800$  lbf/in

Table 2.3: Model data for the single-disk rotor

Station Number	Station length (mm)	Out diameter (mm)	Stiffness Out. Diameter (mm)
1	6.4	22.2	22.2
2	12.7	9.5	9.5
3	12.7	9.5	9.5
4	19.1	9.5	9.5
5	6.4	9.5	9.5
6	12.7	9.5	9.5
7	12.7	9.5	9.5
8	12.7	9.5	9.5
9	12.7	9.5	9.5
10	12.7	9.5	9.5
11	12.7	9.5	9.5
12	12.7	9.5	9.5
13	12.7	9.5	9.5
14	6.4	9.5	9.5
15	19.1	76.2	12.7
16	19.1	9.5	9.5
17	12.7	9.5	9.5
18	3.0	9.5	9.5
19	47.8	34.3	17.8
20	19.1	9.5	9.5
21	12.7	9.5	9.5
22	12.7	9.5	9.5
23	12.7	9.5	9.5
24	12.7	9.5	9.5
25	6.4	9.5	9.5
26	47.8	34.3	17.8
27	5.6	9.5	9.5
28	6.4	9.5	9.5
29	3.8	9.5	9.5
30	6.4	9.5	9.5
31	6.4	9.5	9.5
32	12.7	9.5	9.5
33	12.7	9.5	9.5
34	6.4	9.5	9.5
35	6.4	9.5	9.5

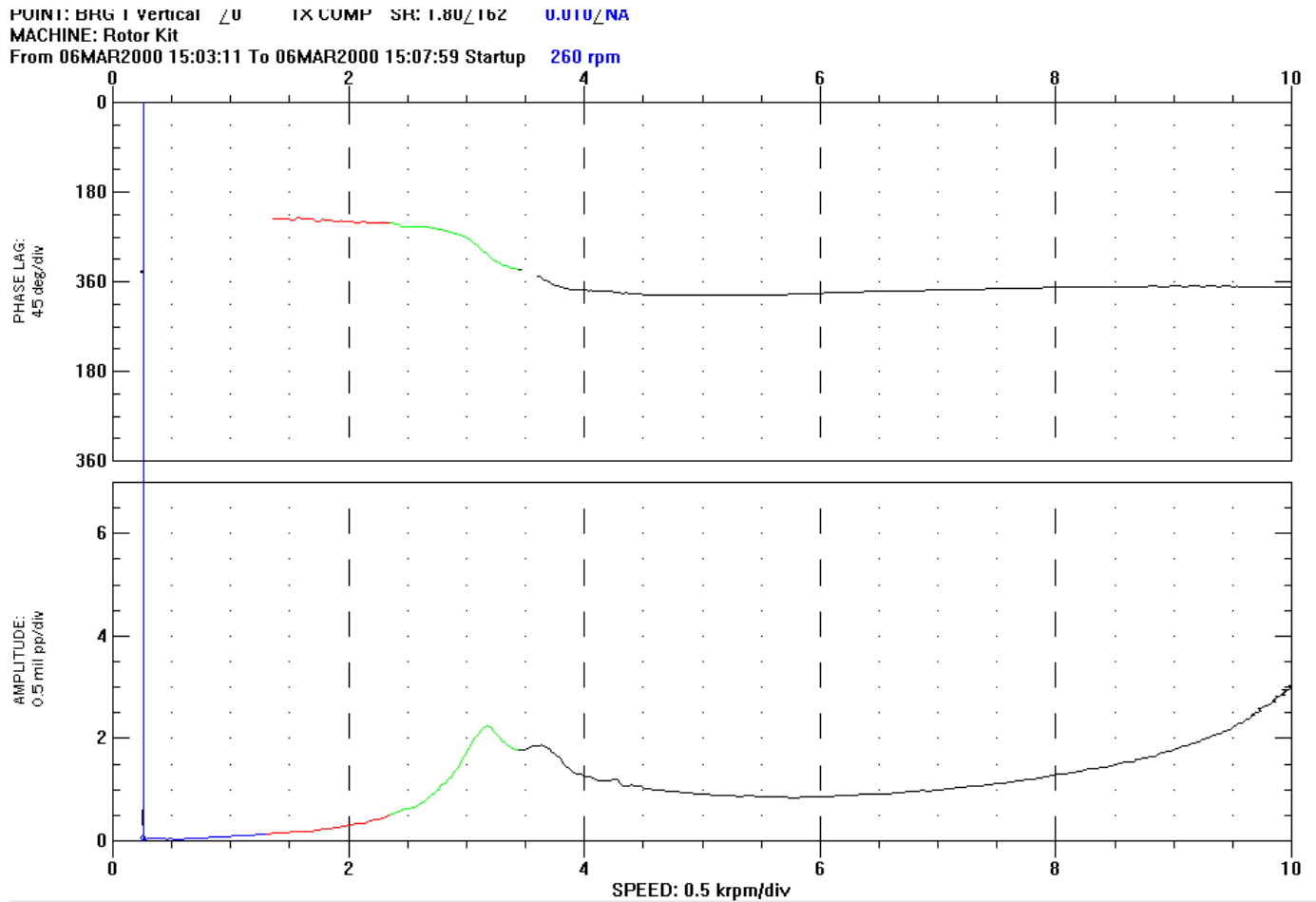


Figure 2.11: Bode Plot of the single-disk rotor supported on its conventional bearings with the AMDs off

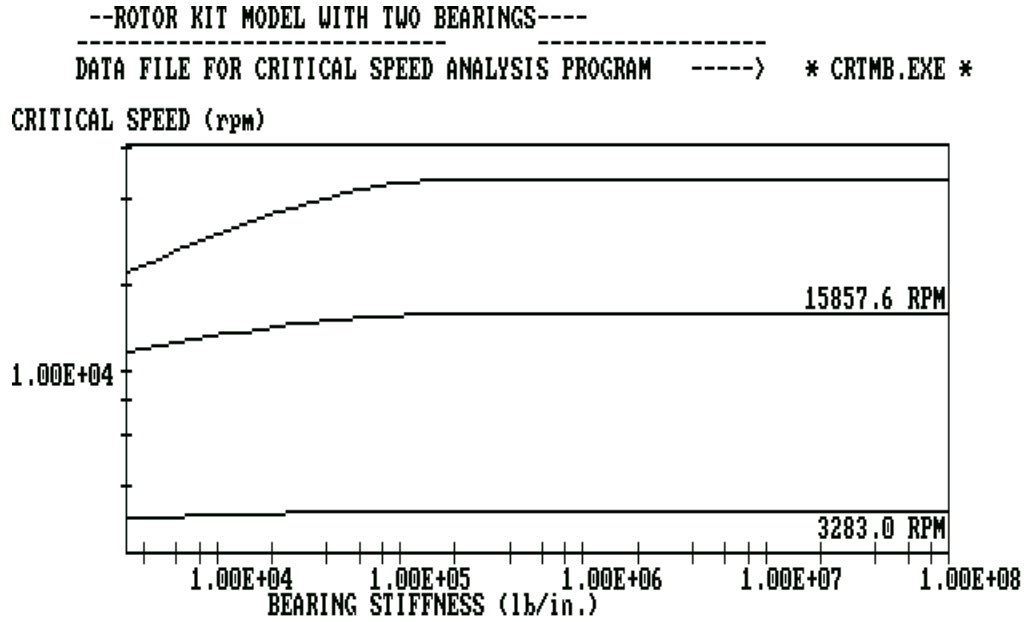


Figure 2.12: Critical speed map of the single-disk rotor supported on its conventional bearings with the AMDs off.  $K_{FFB}=1800$  lbf/in

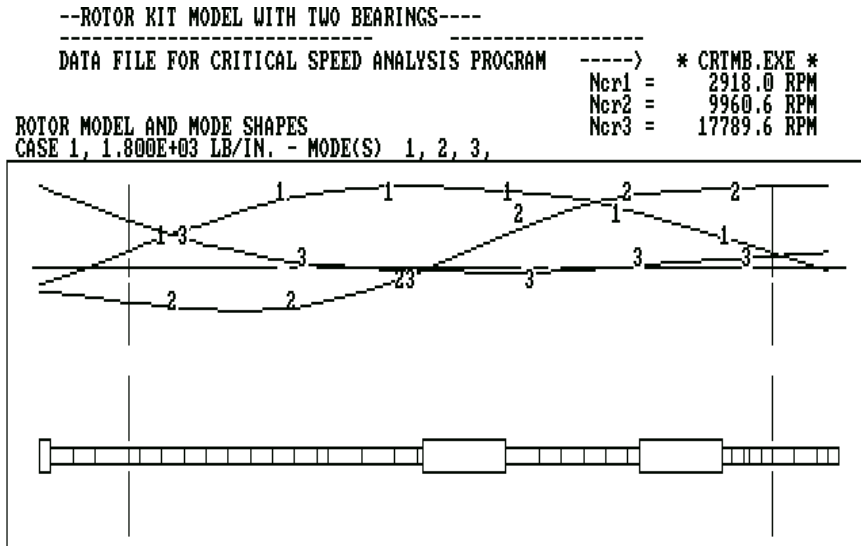


Figure 2.13: Mode shapes of the single-disk rotor supported on its conventional bearings with the AMDs off.  $K_{FFB}=1800$  lbf/in

#### 2.4.1.2 Rotor with the AMD-13 on

A third bearing was added to the previous rotor model at station 19 as shown in Figure 2.14 to account for the effect of turning the AMD-13 on. The fluid film bearing stiffness was again considered to be 1800 lbf/in. The equivalent stiffness associated with the AMD-13 was calculated, as 1470 lbf/in, but it was determined that a stiffness of 800 lbf/in, produced a better match with the experimental results. Figure 2.15 shows the undamped critical speed map. The calculated undamped first critical speed is 4421 RPM (73.68 Hz). This value is within 15.8% of the measured damped critical speed, 5120 RPM (85.3 Hz). Figure 2.16 shows the mode shapes for the first, second and third critical speeds. The Bode plot obtained experimentally using ADRE is shown in Figure 2.17. The first undamped critical speed for the single-disk rotor supported on its conventional bearings is 2918 RPM (48.6 Hz), which means that the AMD-13 added stiffness to the system, moving the first critical speed to a higher frequency of 5120 RPM (85.3 Hz).

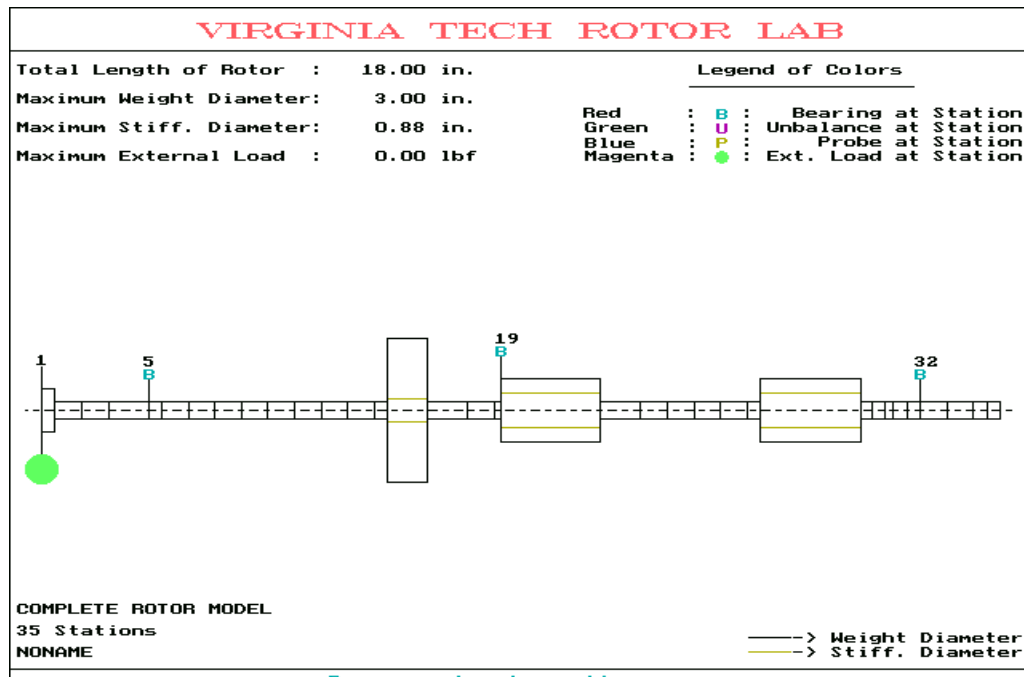


Figure 2.14: VT Fast graphic model of the single-disk rotor supported on its conventional bearings and the AMD-13.  $K_{FFB}=1800$  lbf/in ;  $K_{AMD-13}=800$  lbf/in

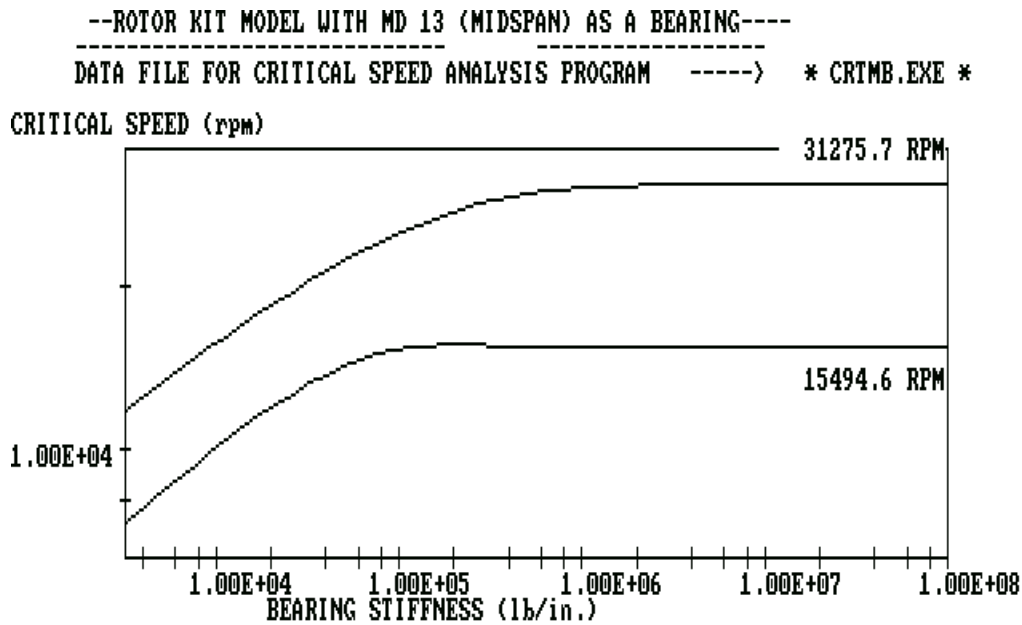


Figure 2.15: Critical speed map for the single-disk rotor supported on its conventional bearings and the AMD-13.  $K_{FFB}=1800$  lbf/in ;  $K_{AMD-13}=800$  lbf/in

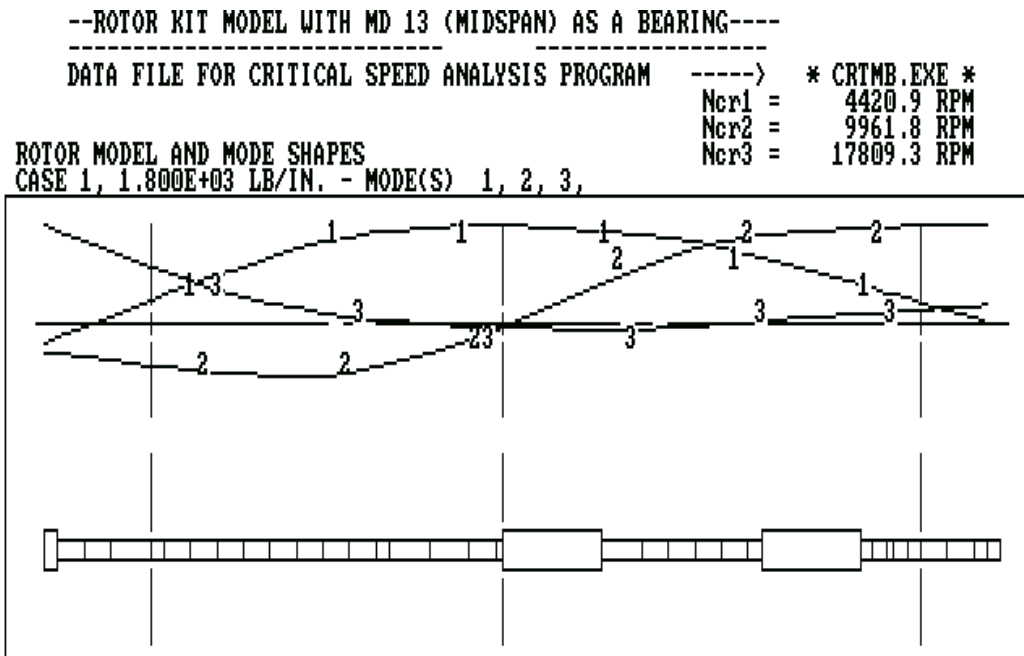


Figure 2.16: Mode shapes for the single-disk rotor supported on its conventional bearings and the AMD-13.  $K_{\text{FFB}}=1800 \text{ lbf/in}$  ;  $K_{\text{AMD-13}}=800 \text{ lbf/in}$



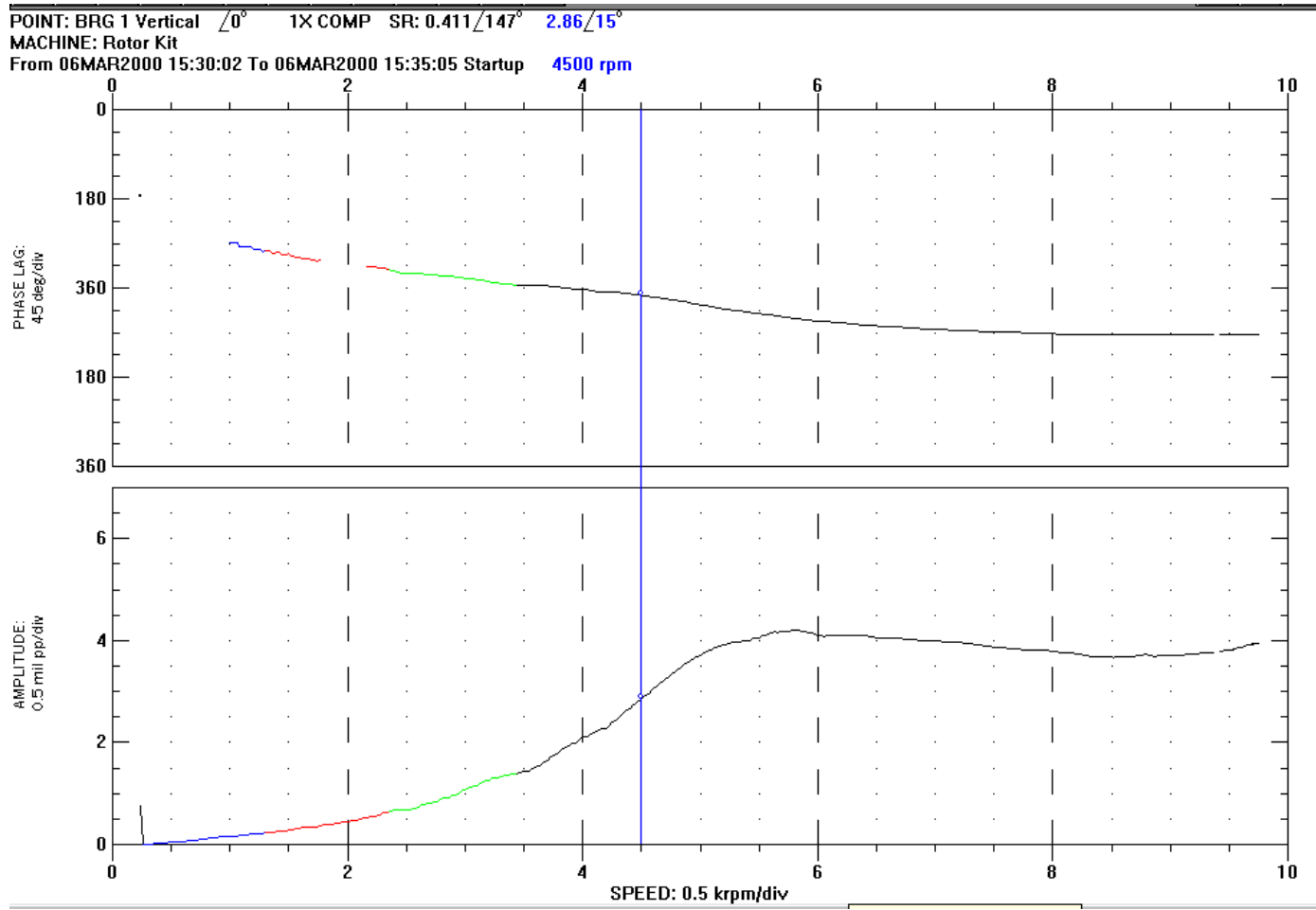


Figure 2.17 : Bode Plot of the single-disk rotor supported on its conventional bearings and the AMD-13

### 2.4.1.3 Rotor with the AMD-24 on

A third bearing was added to the model of the single-disk rotor supported on its conventional bearings at station 26 as shown in Figure 2.18 to mimic the effect of the AMD-24. The fluid film bearing stiffness was again considered as 1800 lbf/in. The stiffness of the AMD-24 was again estimated to be 800 lbf/in. Figure 2.19 shows the undamped critical speed map. The calculated undamped first critical speed is 3514 RPM (58.6 Hz). This value is within 10.4 % of the damped critical speed, 3880 RPM (64.7 Hz), obtained experimentally using ADRE. Figure 2.20 shows the mode shapes for the first, second and third critical speeds, and Figure 2.21 shows the bode plot for this configuration. The first undamped critical speed for this configuration is now at a higher frequency with respect to the configuration of the single-disk rotor supported on its conventional bearings, 2918 RPM (48.6 Hz), due to the added stiffness to the system with the addition of AMD-24.

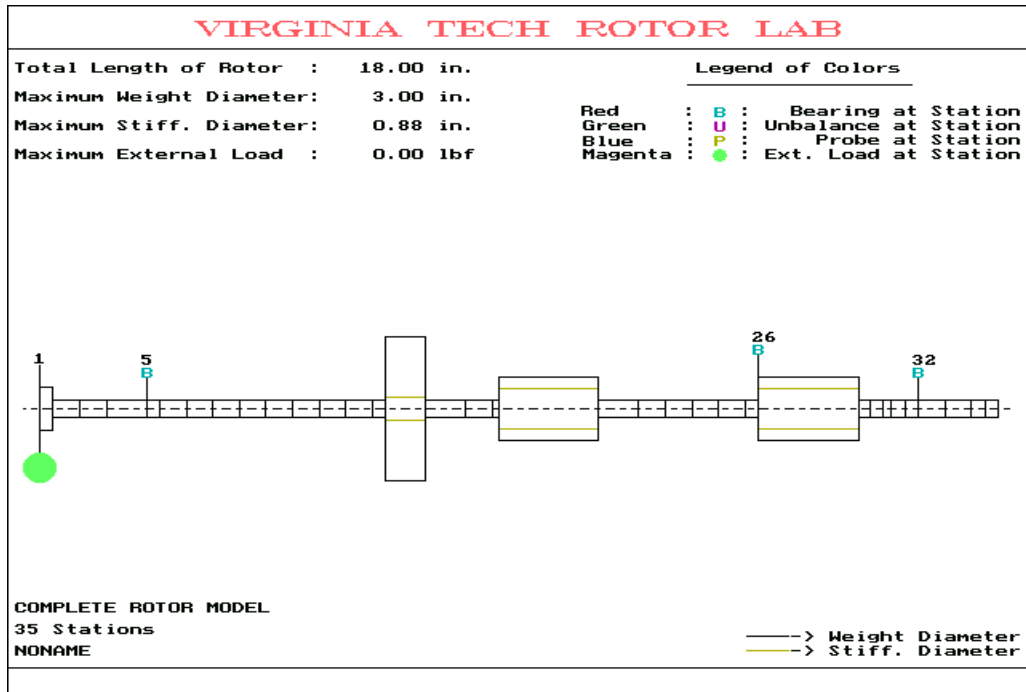


Figure 2.18: VT Fast graphic model for the single-disk rotor supported on its conventional bearings and the AMD-24.  $K_{FFB}=1800$  lbf/in ;  $K_{AMD-24}=800$  lbf/in

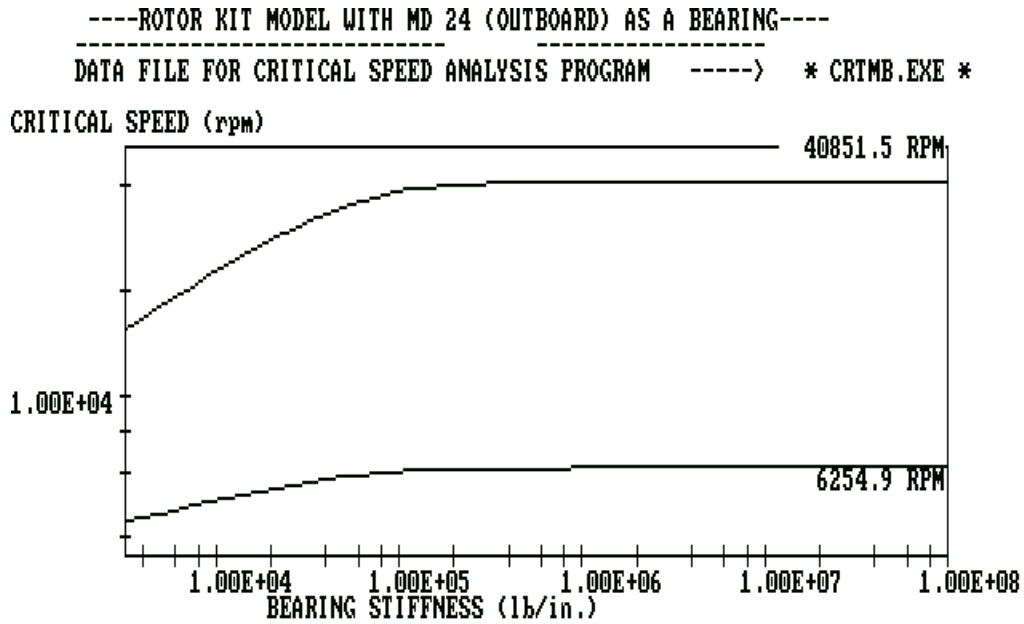


Figure 2.19: Critical speed map of the single-disk rotor supported on its conventional bearings and the AMD-24.  $K_{FFB}=1800$  lbf/in ;  $K_{AMD-24}=800$  lbf/in

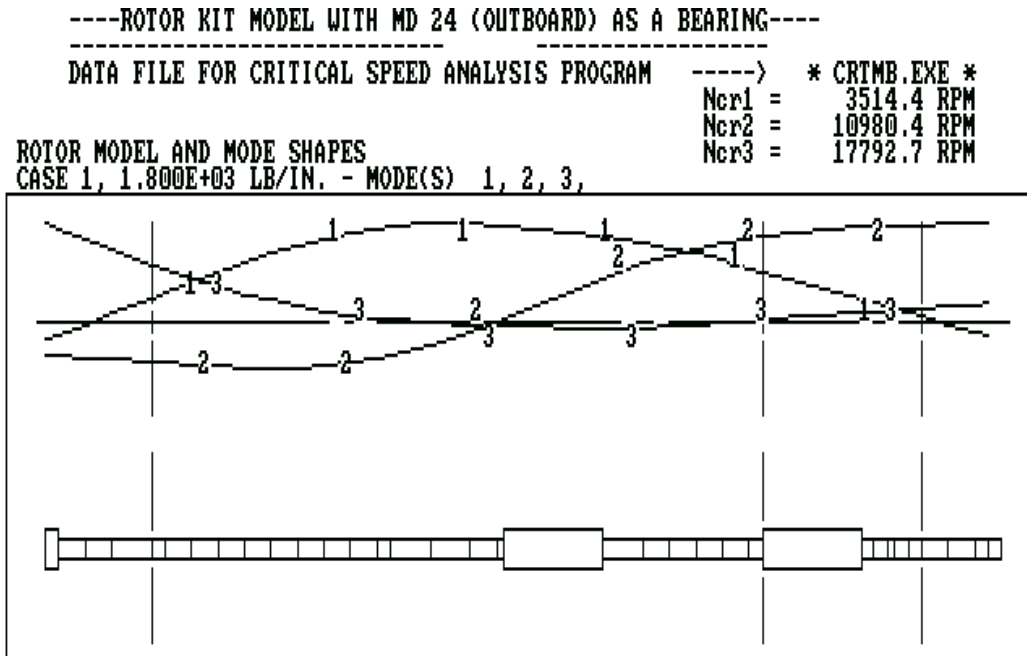


Figure 2.20: Mode shapes of the single-disk rotor supported on its conventional bearings and the AMD-24.  $K_{FFB}=1800$  lbf/in ;  $K_{AMD-24}=800$  lbf/in

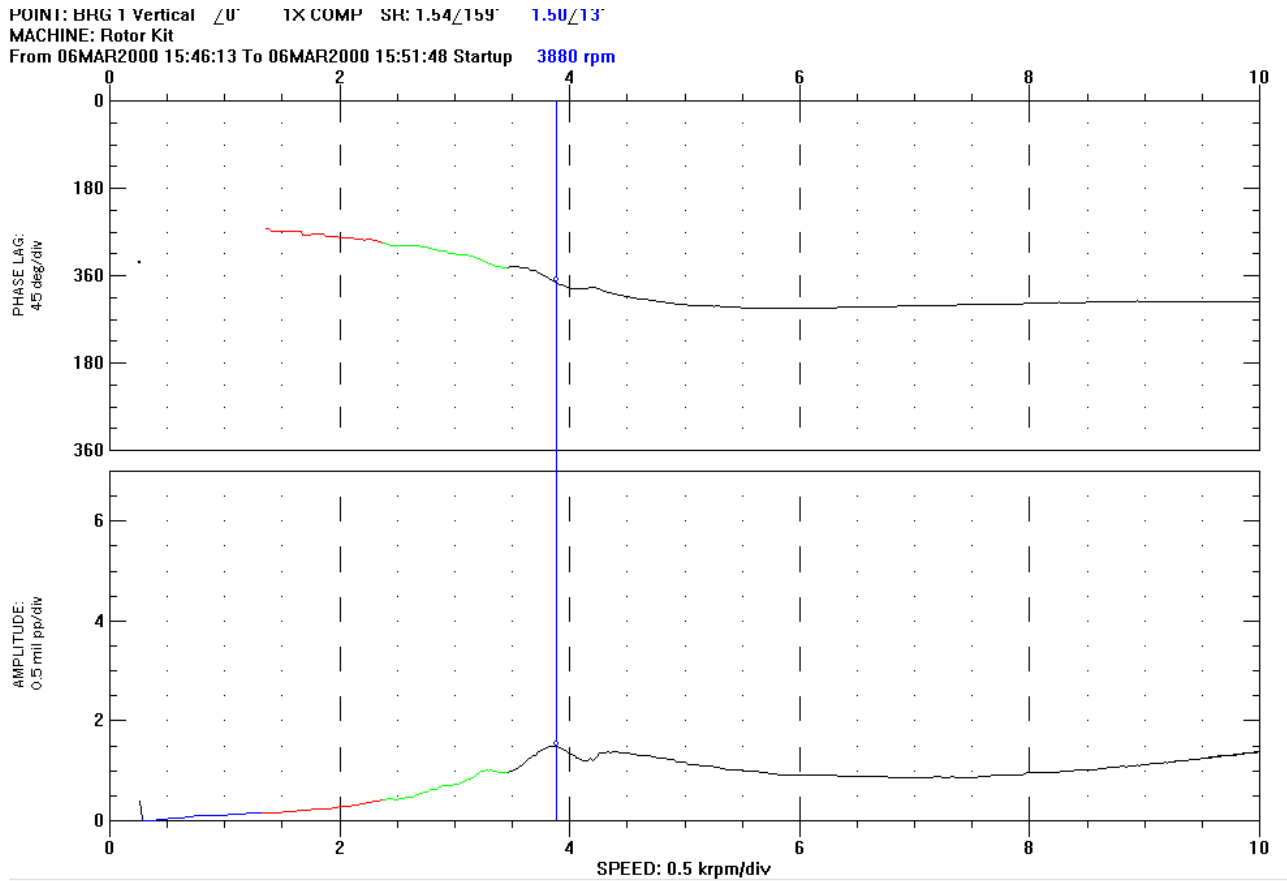


Figure 2.21 Bode plot of the single-disk rotor supported on its conventional bearings and the AMD-24

## 2.4.2 Three-Disk Rotor Critical Speeds

Three different configurations were considered for the three-disk rotor. The first one corresponded to the rotor supported on its conventional bearings and the AMDs off as shown in Figure 2.22. In order to study the effect that turning the AMDs on would have on the dynamics of the rotor, two more configurations were analyzed. One considering the AMD at a quarter-span (AMD-24) as a third bearing or damper, shown in Figure 2.23, and another one considering the AMD at two-thirds of the rotor span (AMD-13) as a third bearing or damper, shown in Figure 2.24.

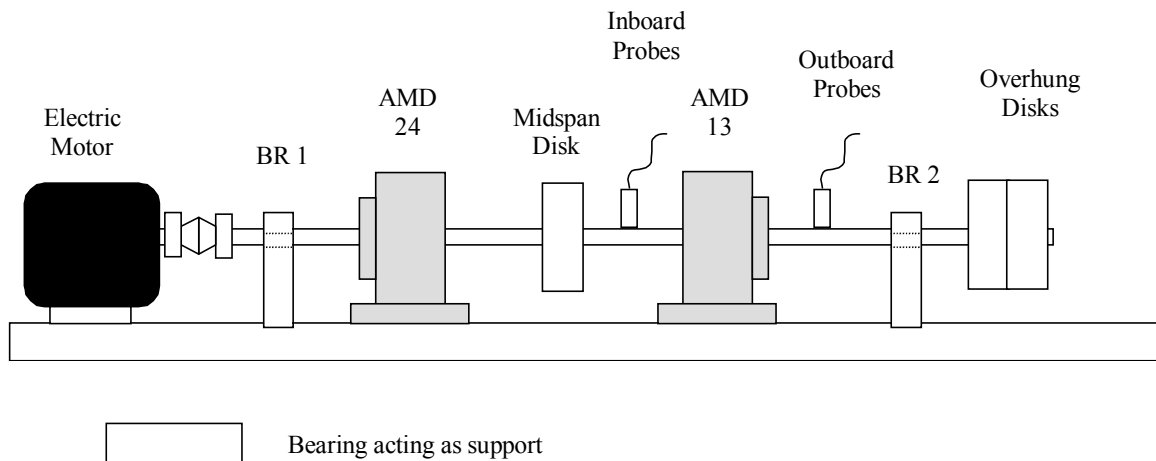


Figure 2.22: Schematic showing the three-disk rotor supported on its conventional bearings (not to scale)

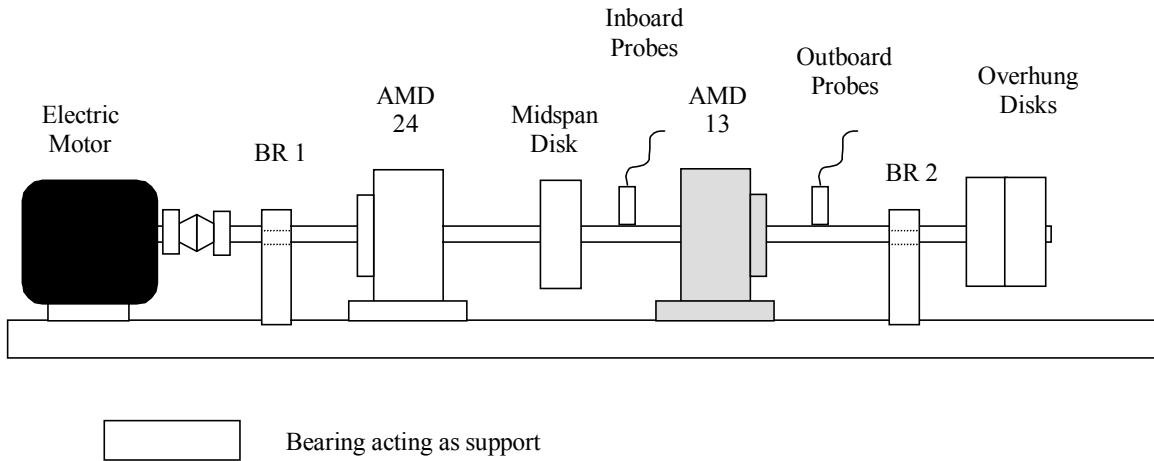


Figure 2.23: Schematic showing the three-disk rotor supported on its conventional bearings and the AMD-24 (not to scale)

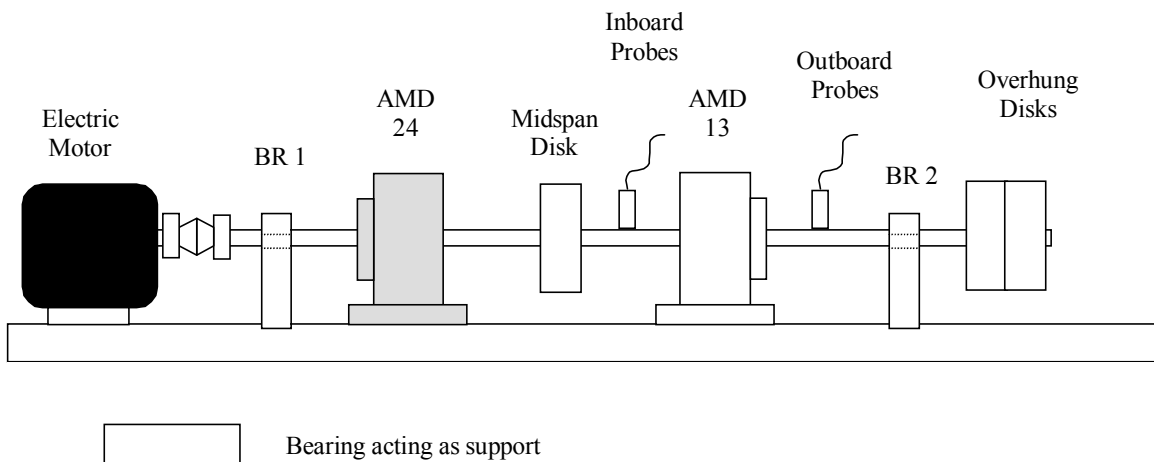


Figure 2.24: Schematic showing the three-disk rotor supported on its conventional bearings and the AMD-24 (not to scale)



Table 2.4: Model data for the three-disk rotor

Station Number	Station length (mm)	Out diameter (mm)	Stiffness Out. Diameter (mm)
1	6.4	22.2	10.0
2	63.5	9.5	9.5
3	12.7	9.5	9.5
4	92.7	9.5	9.5
5	47.8	34.3	12.7
6	82.3	9.5	9.5
7	25.4	76.2	21.6
8	92.1	9.5	9.5
9	47.8	34.3	12.7
10	55.9	9.5	9.5
11	12.7	9.5	9.5
12	57.2	9.5	9.5
13	19.1	76.2	21.6
14	19.1	76.2	21.6
15	3.2	9.5	9.5

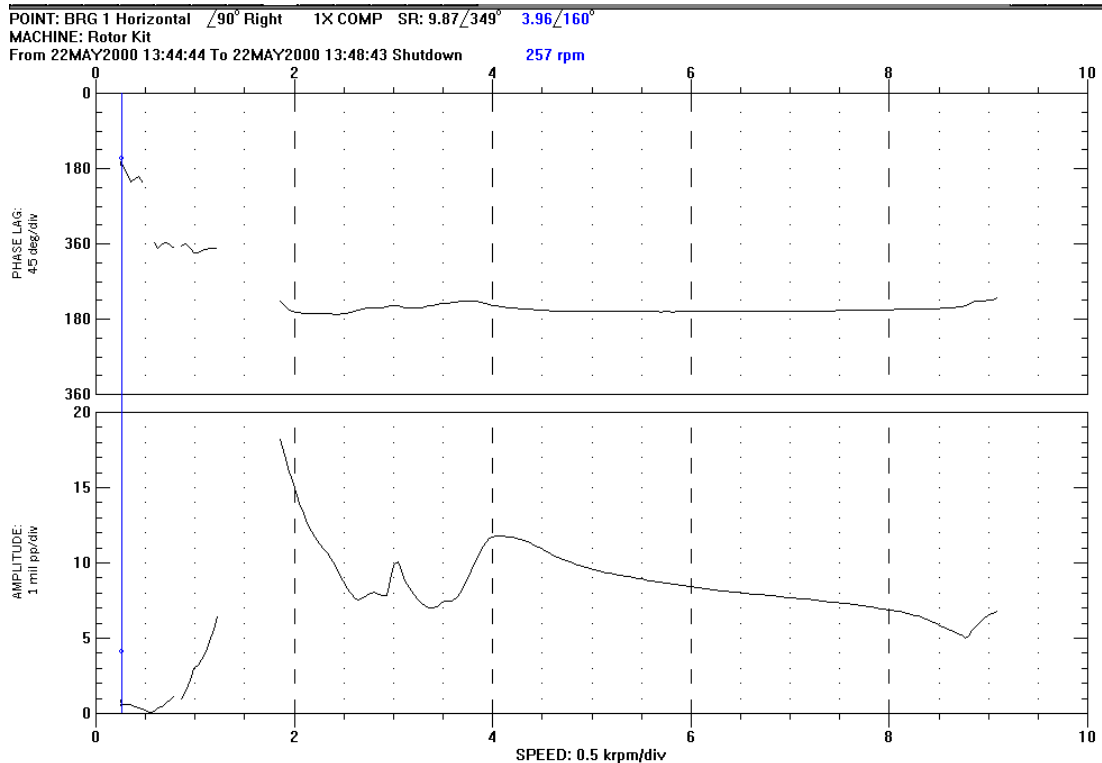


Figure 2.26: Bode Plot of the three-disk rotor supported on its conventional bearings with the AMDs off



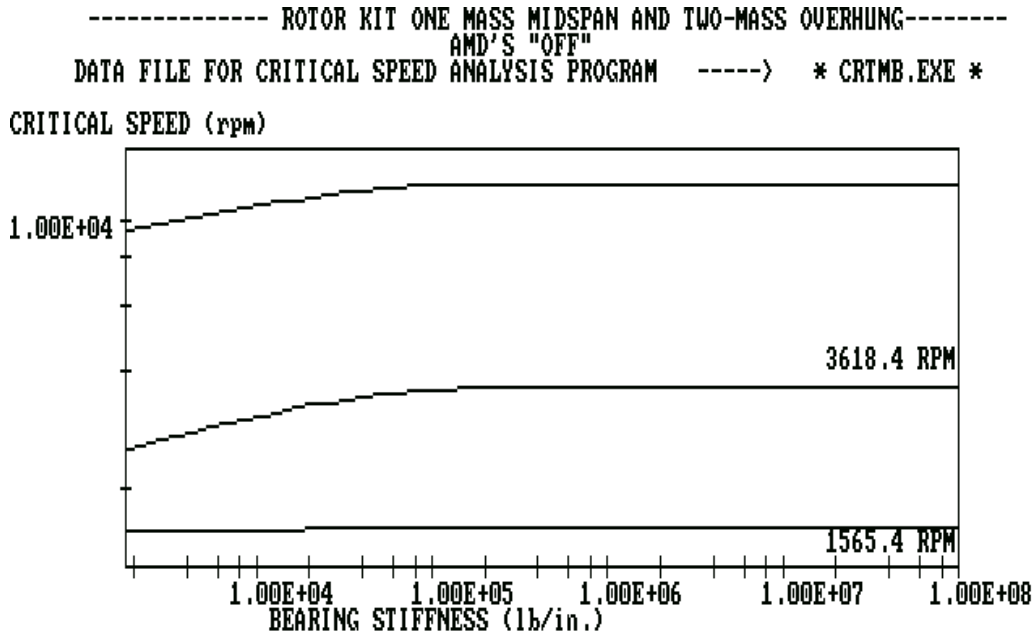


Figure 2.27: Critical speed map of the three-disk rotor supported on its conventional bearings with the AMDs off.  $K_{FFB}=1800$  lbf/in

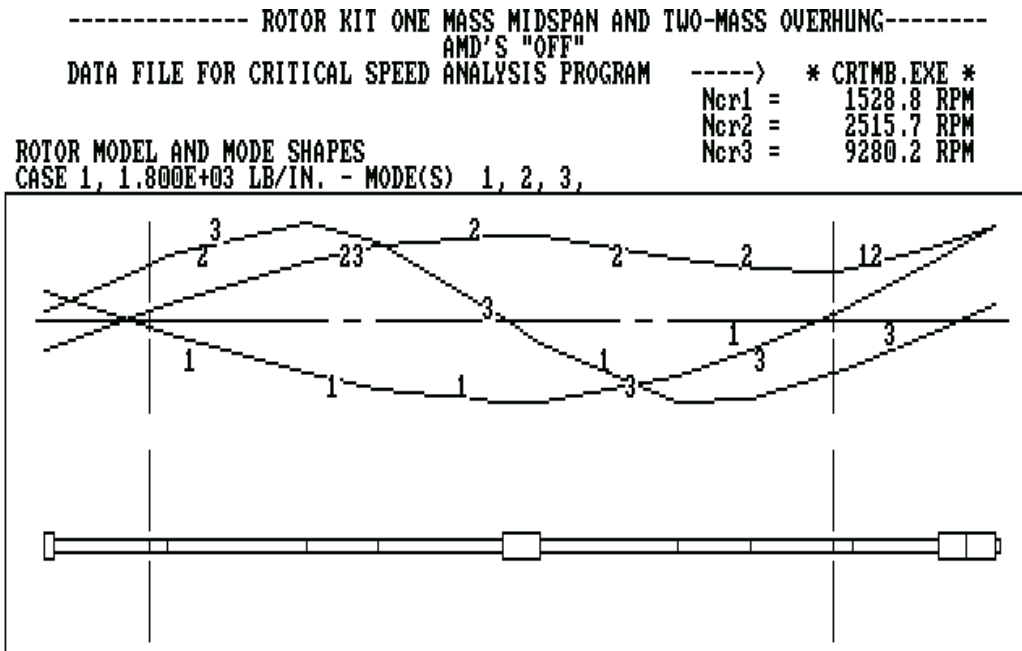


Figure 2.28: Mode shapes of the three-disk rotor supported on its conventional bearings with the AMDs off.  $K_{FFB}=1800$  lbf/in

### 2.4.2.2 Rotor with the AMD-24 on

A third bearing was added to the previous rotor model at station five as shown in Figure 2.29 to account for the effect of turning the AMD-24 on. The fluid film support bearing stiffness was again approximated as 1800 lb/in and was considered constant with the speed. The equivalent stiffness associated with the AMD-13 was calculated, to be 1470 lbf/in, but it was determined that a stiffness of 800 lbf/in produced a better match with the experimental results. Figure 2.30 shows the undamped critical speed map. The calculated undamped first critical speed is 1834 RPM (30.6 Hz). This value is within 8% of the measured damped critical speed, 1980 RPM (33 Hz). Figure 2.31 shows the mode shapes for the first, second and third critical speeds. The Bode plot obtained experimentally using ADRE is shown in Figure 2.32. The calculated first undamped critical speed for the three-disk rotor supported on its conventional bearings is 1529 RPM (25.48 Hz), which means that the AMD-24 did not produce a significant change in the dynamics of the three-disk rotor. The calculated second critical speed is 2931 RPM (48.9 Hz), this value is about 33% below the measured damped second critical speed, 4400 RPM (73.3 Hz). The difference between the calculated and the measured second critical speed is probably due to a change in the fluid film bearing stiffness with the speed.

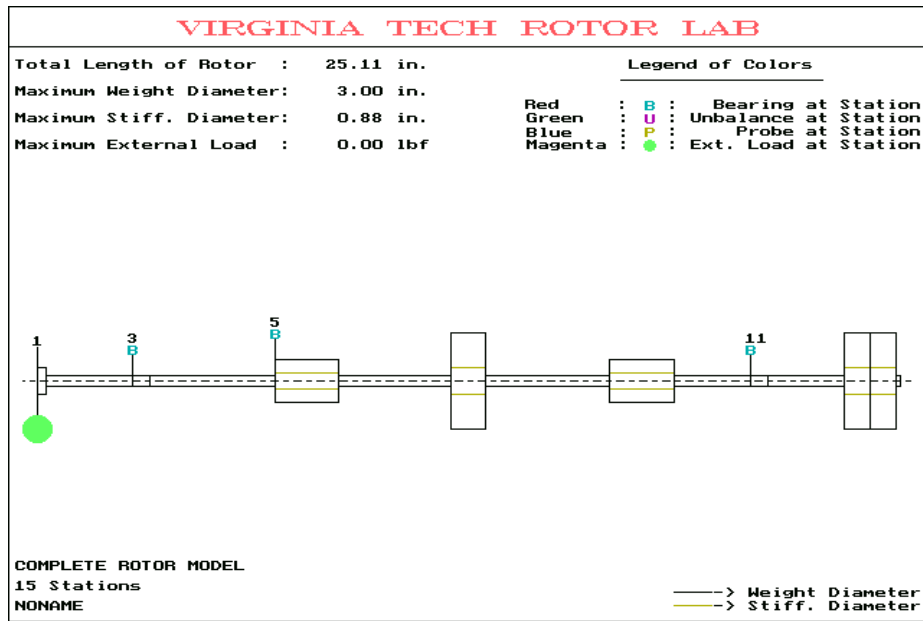


Figure 2.29: VT Fast graphic model of the three-disk rotor supported on its conventional bearings and the AMD-24.  $K_{FFB}=1800$  lbf/in ;  $K_{AMD-24}=800$  lbf/in

----- ROTOR KIT ONE MASS MIDSPAN AND TWO-MASS CATILIVER-----  
 AMD-24 (INBOARD) AS A THIRD BEARING AMD-13 (OUTBOARD) "  
 DATA FILE FOR CRITICAL SPEED ANALYSIS PROGRAM -----> \* CRTMB.EXE \*

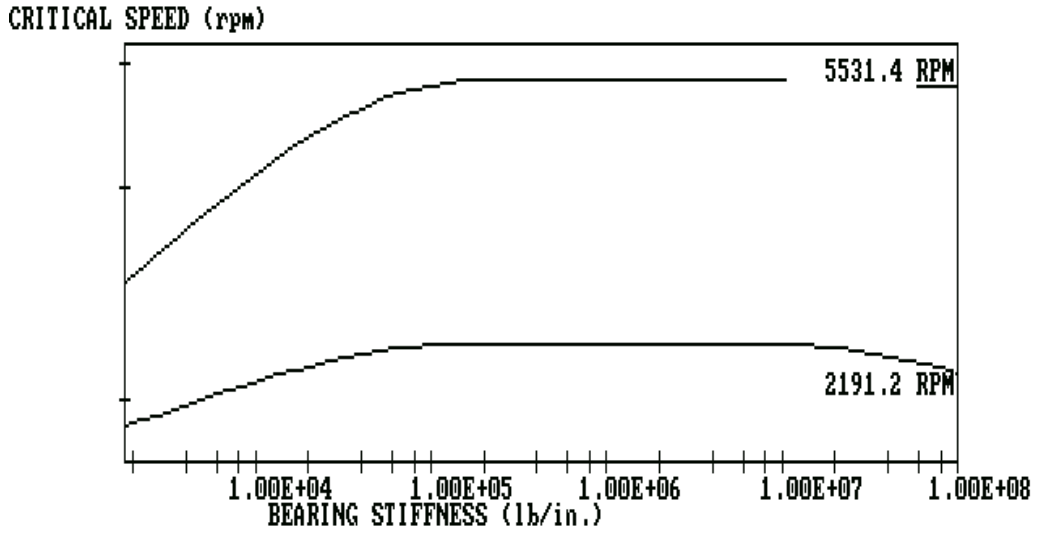


Figure 2.30: Critical speed map for the three-disk rotor supported on its conventional bearings and the AMD-24.  $K_{FFB}=1800$  lbf/in ;  $K_{AMD-24}=800$  lbf/in

----- ROTOR KIT ONE MASS MIDSPAN AND TWO-MASS CATILIVER-----  
 AMD-24 (INBOARD) AS A THIRD BEARING AMD-13 (OUTBOARD) "  
 DATA FILE FOR CRITICAL SPEED ANALYSIS PROGRAM -----> \* CRTMB.EXE \*

Ncr1 = 1834.4 RPM  
 Ncr2 = 2931.3 RPM  
 Ncr3 = 10336.6 RPM

ROTOR MODEL AND MODE SHAPES  
 CASE 1, 1.800E+03 LB/IN. - MODE(S) 1, 2, 3,

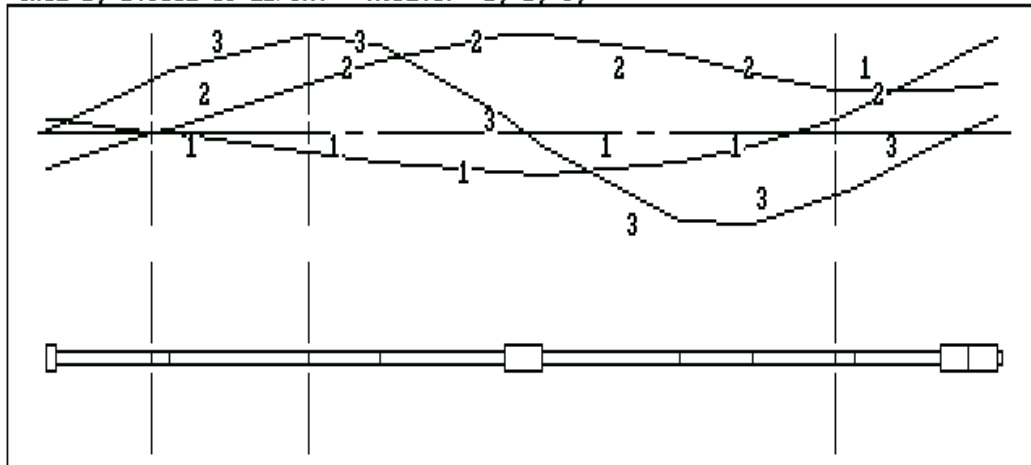


Figure 2.31: Mode shapes for the three-disk rotor supported on its conventional bearings and the AMD-24.  $K_{FFB}=1800$  lbf/in ;  $K_{AMD-24}=800$  lbf/in

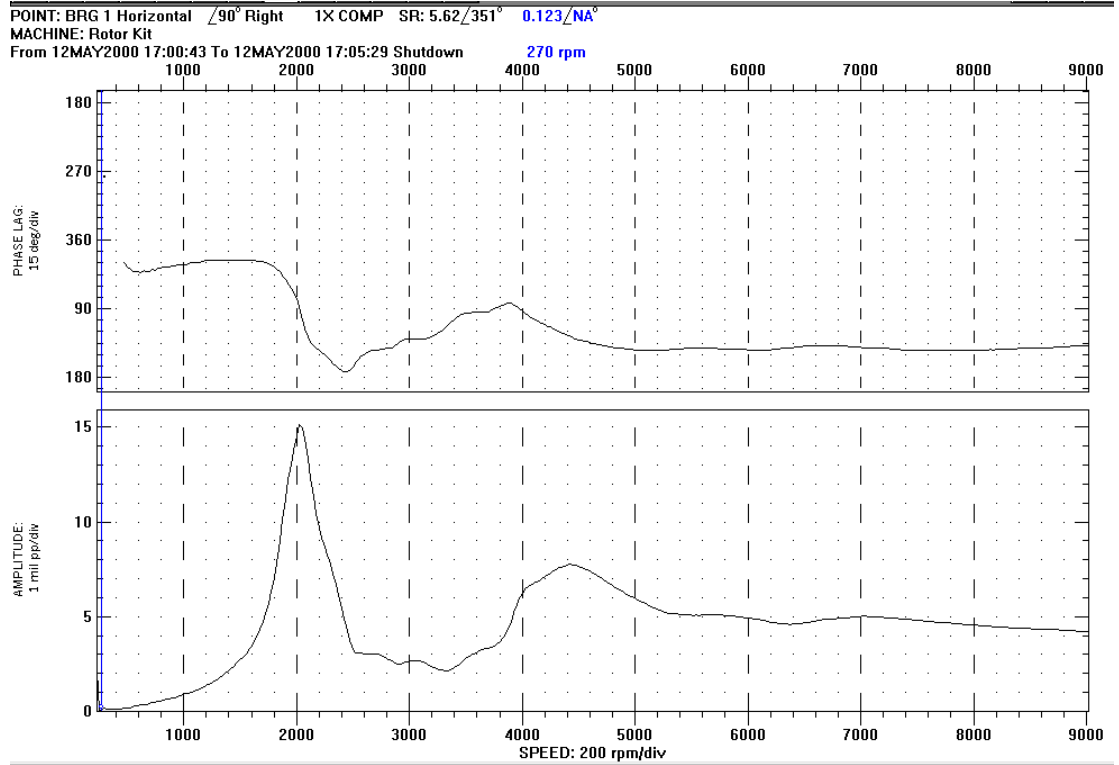


Figure 2.32: Bode Plot of the three-disk rotor supported on its conventional bearings and the AMD-24

### 2.4.2.2 Rotor with the AMD-13 on

A third bearing was added to the model of the three-disk rotor supported on its conventional bearings at station nine as shown in Figure 2.33 to mimic the effect of the AMD-13. The fluid film bearing stiffness was again considered as 1800 lbf/in and constant with the speed. The equivalent stiffness associated with the AMD-13 was again estimated to be 800 lbf/in. Figure 2.34 shows the undamped critical speed map. The calculated undamped first critical speed is 1851 RPM (30.9 Hz). This value is within 16 % of the damped critical speed, 2150 RPM (35.8 Hz), obtained experimentally using ADRE. Figure 2.35 shows the mode shapes for the first, second and third critical speeds, and Figure 2.36 shows the Bode plot for this configuration. The first undamped critical speed for the three-disk rotor supported on its conventional bearings is 1529 RPM (25.48 Hz), which means that the AMD-24 did not produce a significant change in the dynamics of the three-disk rotor. The calculated second critical speed is 2999 RPM (50 Hz), this value is about 23% below the measured damped second critical speed, 3880 RPM (64.7 Hz). The difference between the calculated and the measured second critical speed is probably due to a change in the fluid film bearing stiffness with the speed.

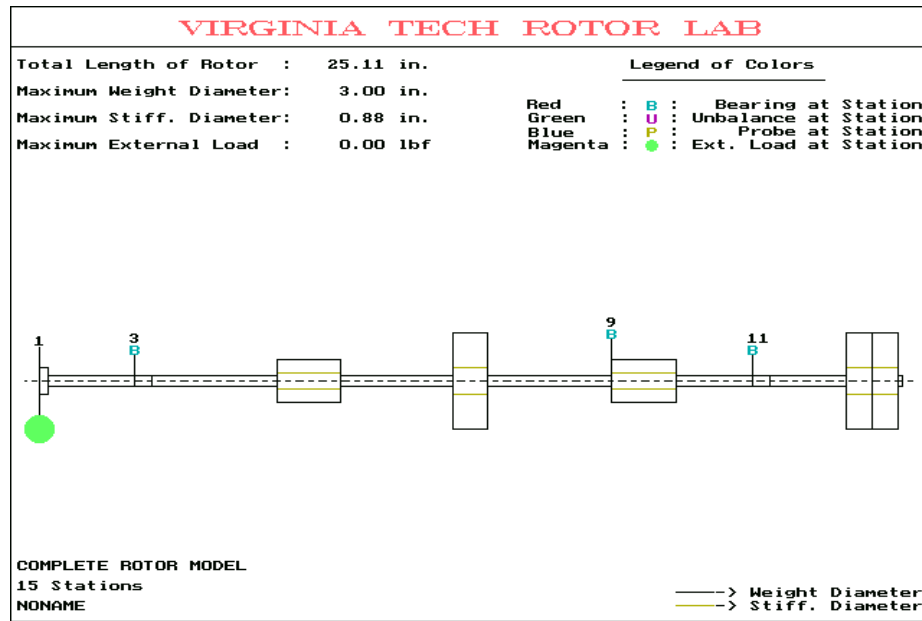


Figure 2.33: VT Fast graphic model for the three-disk rotor supported on its conventional bearings and the AMD-13.  $K_{FFB}=1800$  lbf/in ;  $K_{AMD-13}=800$  lbf/in

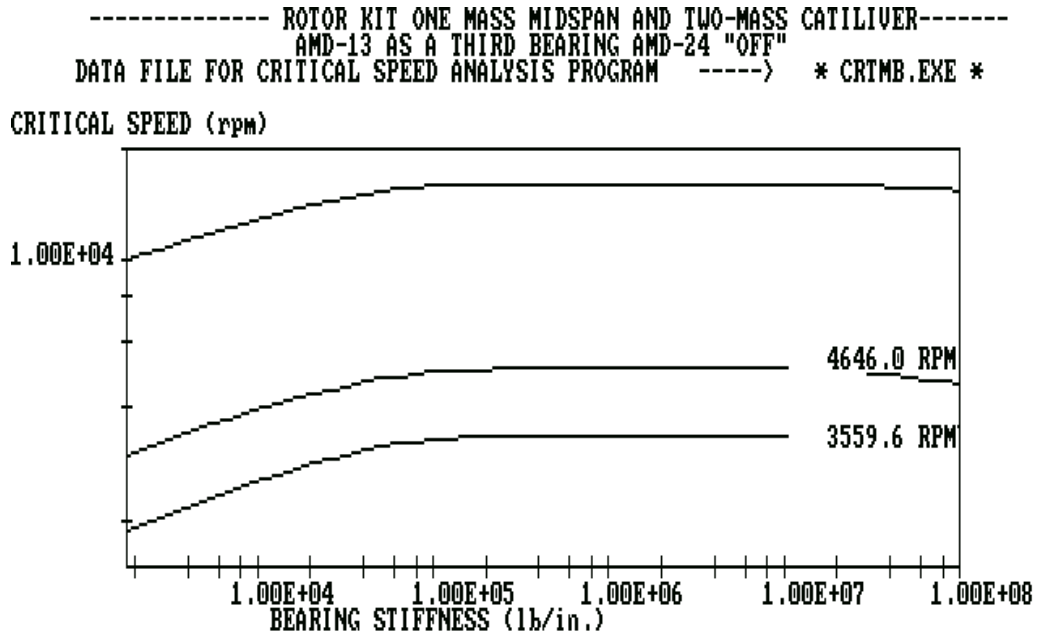


Figure 2.34: Critical speed map of the three-disk rotor supported on its conventional bearings and the AMD-13.  $K_{FFB}=1800$  lbf/in ;  $K_{AMD-13}=800$  lbf/in

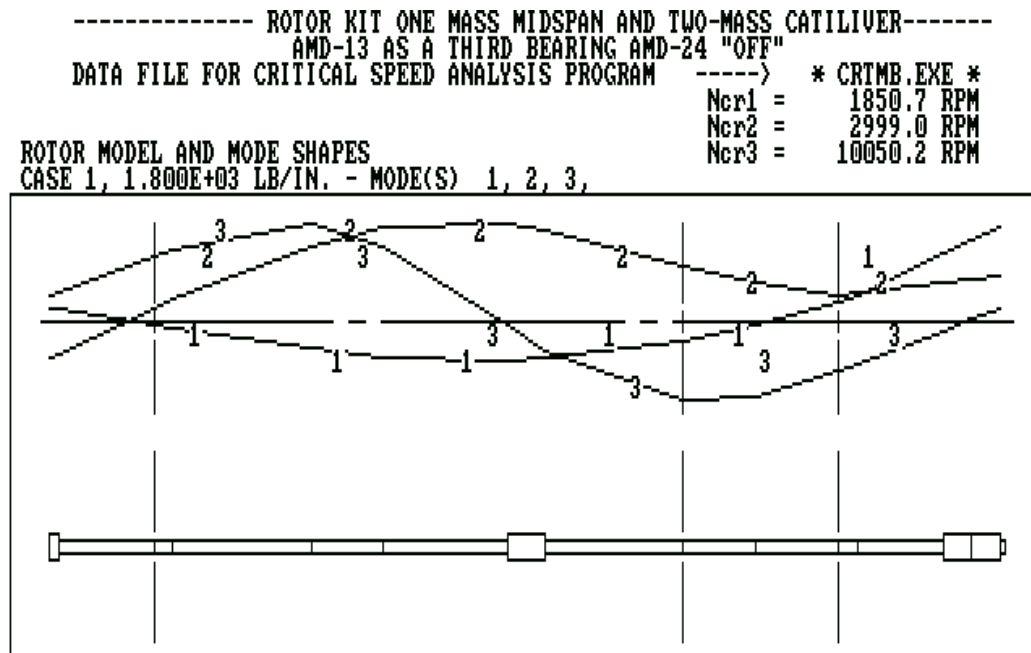


Figure 2.35: Mode shapes of the three-disk rotor supported on its conventional bearings and the AMD-13.  $K_{FFB}=1800$  lbf/in ;  $K_{AMD-13}=800$  lbf/in

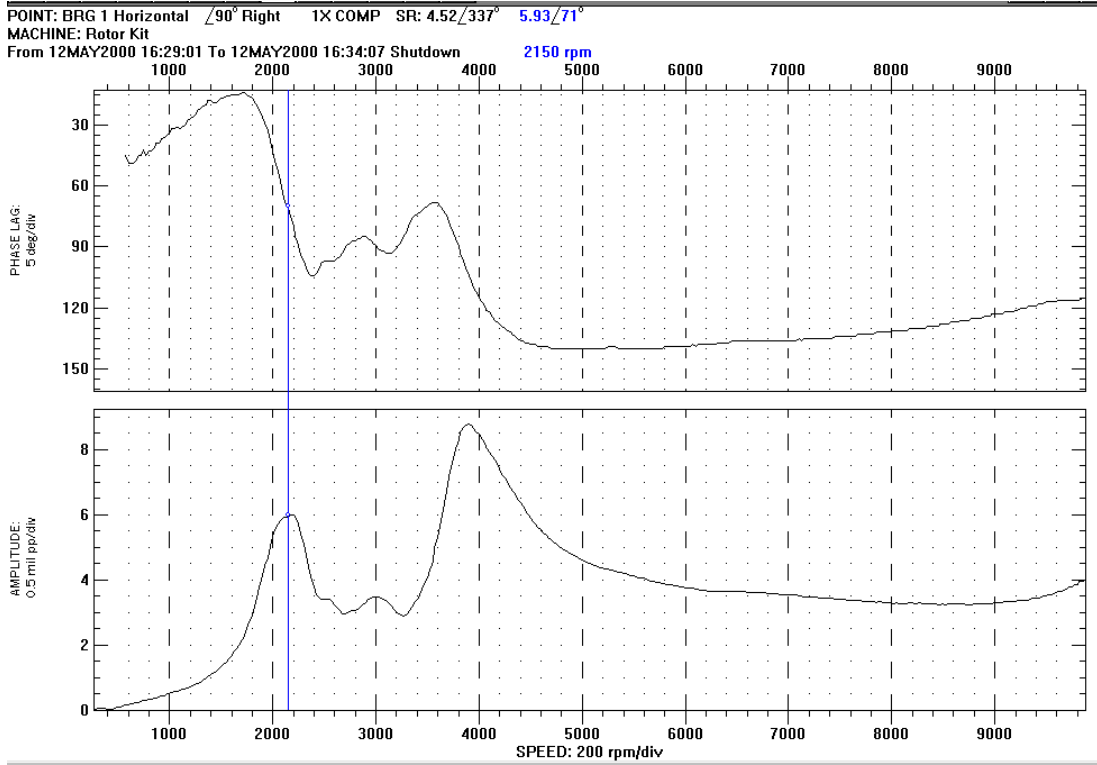


Figure 2.36 Bode plot of the three-disk rotor supported on its conventional bearings and the AMD-13

## **2.5 Forced Response**

Results of the critical speed analysis show how the AMDs add stiffness to the original rotor-bearing system changing the location of the first critical speed to a higher frequency. A forced response analysis was performed in order to investigate the effect that the AMDs would have in the synchronous forced response of the single-disk rotor.

### **2.5.1 Single-Disk Rotor**

#### **2.5.1.1 Rotor with AMDs off**

The model of the single-disk rotor supported on its conventional bearings with the AMDs off for forced response is the same listed in Table 2.2 with the addition of an unbalance of 0.2 gr. placed at the disk (station 15). This model was used as input file in the forced response code (MODLUND) of the Virginia Tech Rotordynamics Laboratory VT Fast program. The fluid film support bearing stiffness is approximated as 1800 lb/in, and the damping was approximated to 8 lb-s/in. Figure 2.37 shows the calculated forced response plot. For this configuration, the response amplitude expected at the first critical speed, 3211 RPM (53.5 Hz) is around 3.00 mils pp, and this agrees with the amplitude obtained experimentally, as shown in the Bode plot of Figure 2.11. The amplification factors obtained from the forced response analysis (7.2) and from the experiments (7.1) are also in agreement. It is important to mention that the actual unbalance of the rotor is unknown and the value considered to perform the forced response analysis (0.2 gr) was estimated at first and was found to match the experimental data.

#### **2.5.1.2 Rotor with the AMD-13 on**

A third bearing was added to the previous rotor model at station 19 to account for the effect of turning the AMD-13 on. A stiffness of 1800 lbf/in and a damping of 8 lbf-s/in were used for the fluid film support bearings characteristics. The equivalent stiffness and damping associated with the AMD-13 were calculated, resulting in 1400 lbf/in and 2.95 lbf-s/in, respectively. These values were introduced in the forced response model but it was found that a stiffness of 700 lbf/in and a damping of 2.0 lbf/in produced a better match with the experimental results. Figure 2.38 shows the calculated forced response plot. For this configuration, the response amplitude expected at the first critical



speed, 5200 RPM (86.7 Hz) is around 3.90 mils pp. The calculated amplitudes agree with the amplitudes obtained experimentally, as shown in the Bode plot of Figure 2.17.

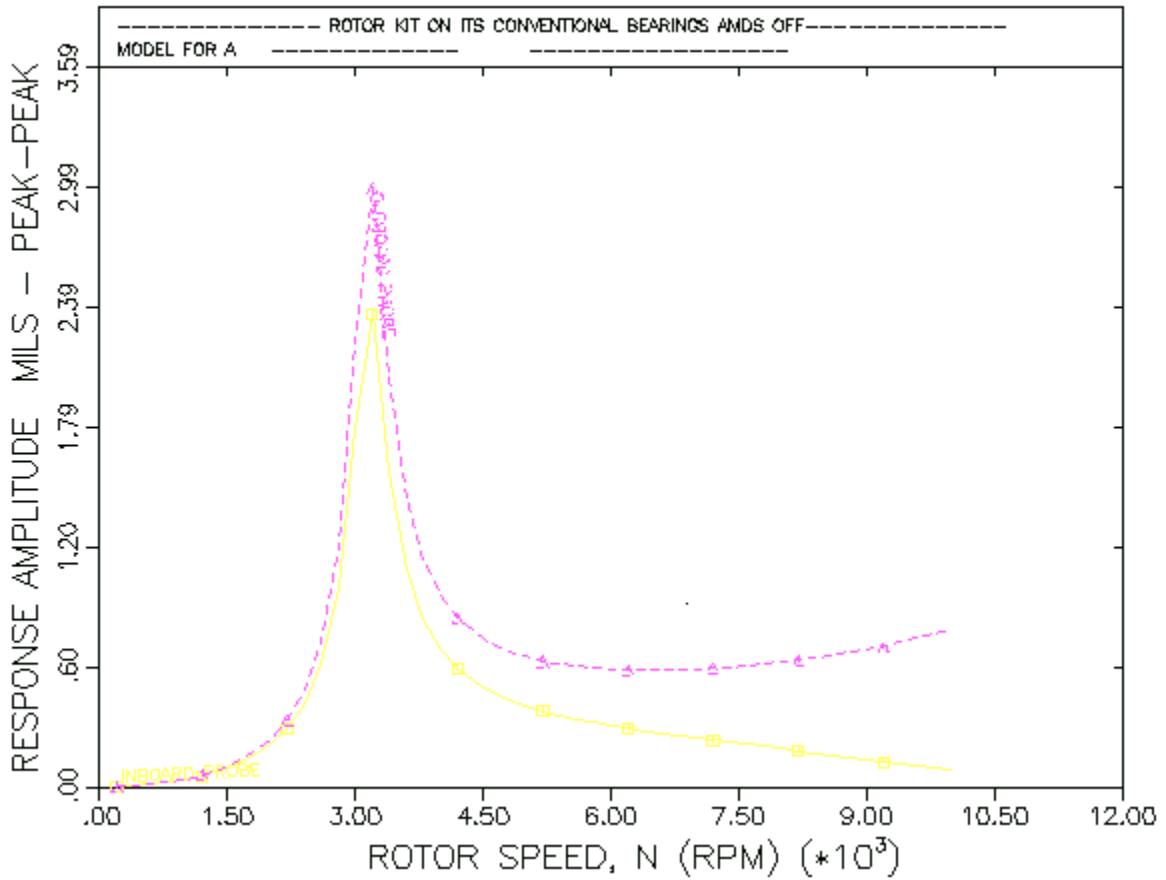


Figure 2.37: Forced response of the single-disk rotor supported on its conventional bearings with the AMDs off. Fluid film support bearing  $K=1800$  lbf/in;  $C=8$  lbf-s/in

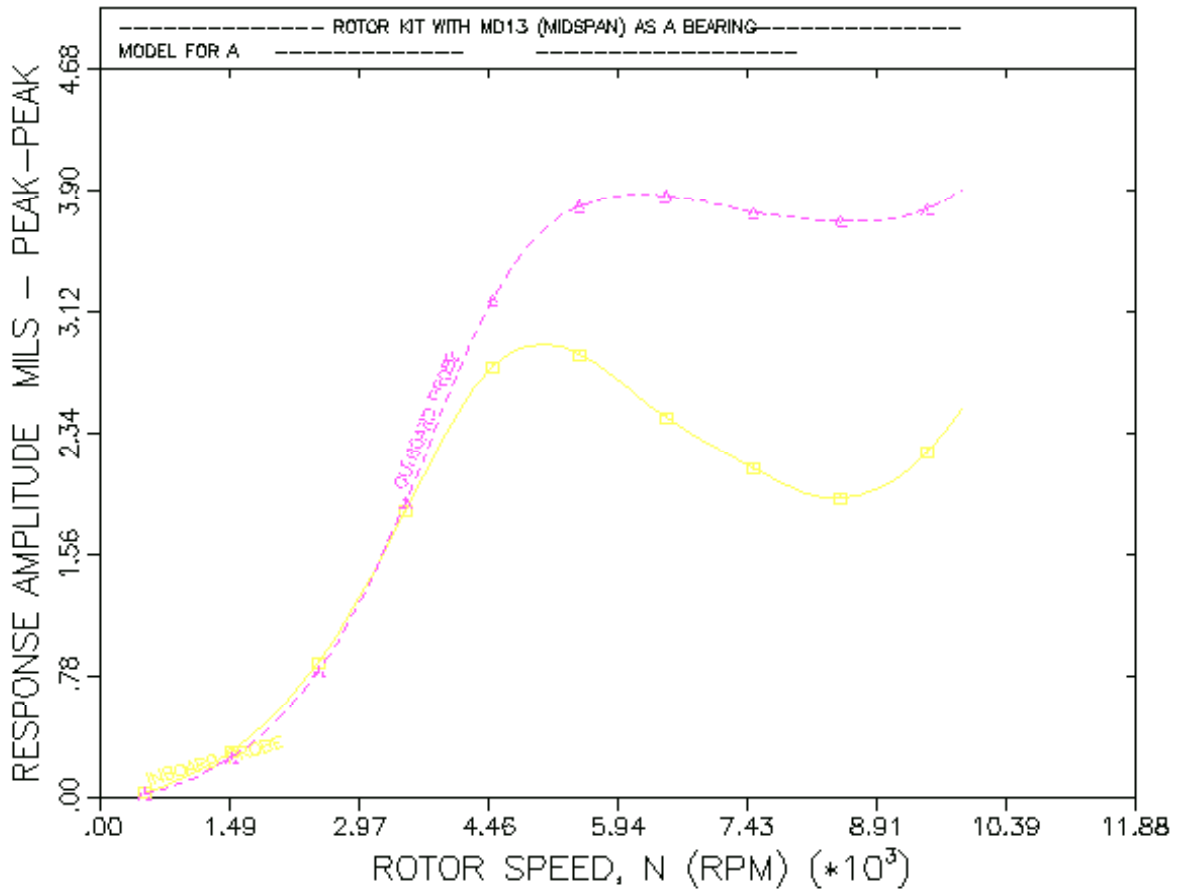


Figure 2.38: Forced response of the single-disk rotor supported on its conventional bearings and the AMD-13. Fluid film support bearings  $K=1800$  lbf/in;  $C=8$  lbf-s/in;  $K_{AMD-13}=700$  lbs/in;  $C_{AMD-13}=2.0$  lbf-s/in

### 2.5.1.3 Rotor with the AMD-24 on

A third bearing was added to the previous rotor model at station 26 to account for the effect of turning the AMD-24 on. A stiffness of 1800 lbf/in and a damping of 8 lbf-s/in were used for the fluid film support bearings characteristics. The equivalent stiffness and damping associated with the AMD-13 were calculated, resulting in 1400 lbf/in and 2.95 lbf-s/in, respectively. These values were introduced in the forced response model but it was found that a stiffness of 700 lbf/in and a damping of 1.2 lbf/in produced a better match with the experimental results. Figure 2.39 shows the calculated forced response plot. For this configuration, the response amplitude expected at the first critical speed, 3705 RPM (61.8 Hz) is around 1.6 mils pp. The calculated amplitudes agree with the amplitudes obtained experimentally, as shown in the Bode plot of Figure 2.21.

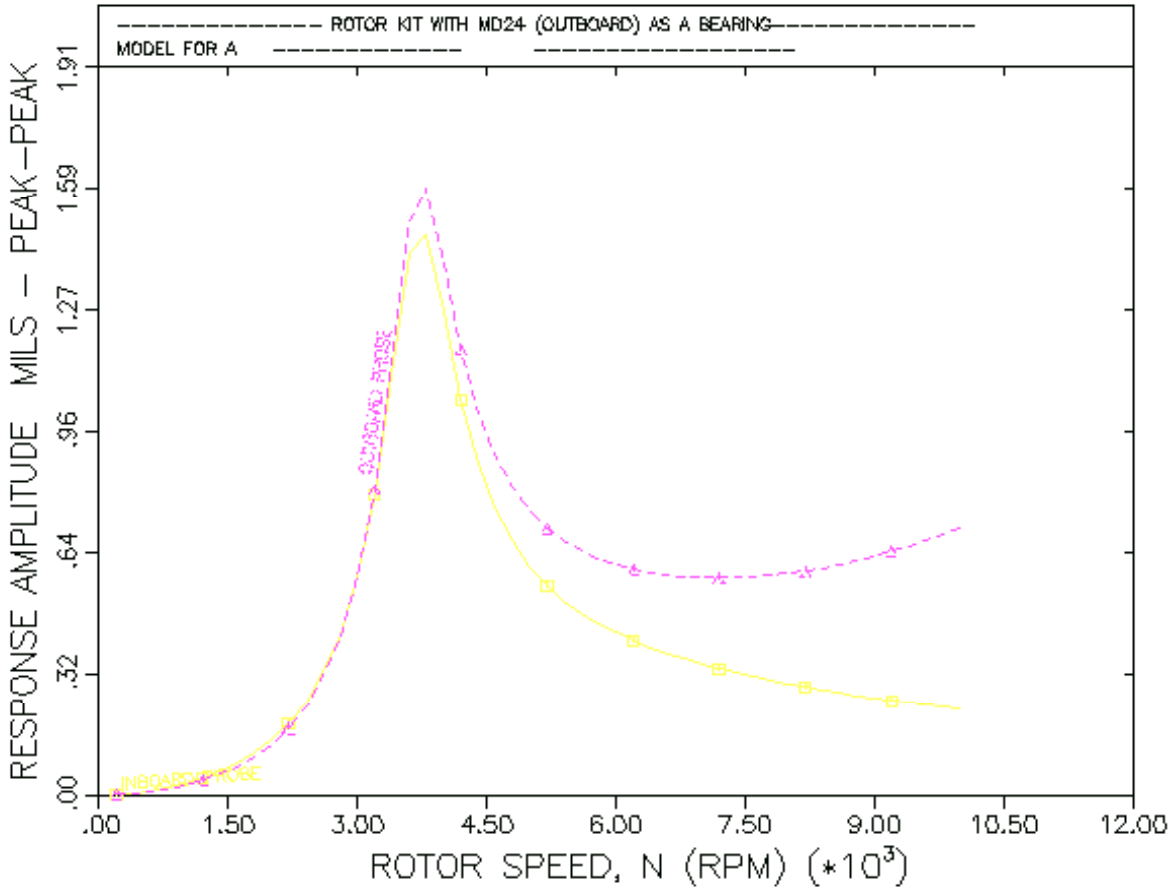


Figure 2.39: Forced response of the single-disk rotor supported on its conventional bearings and the AMD-24.  $K=1800$  lbf/in;  $C=8$  lbf-s/in;  $K_{AMD-24}=700$  lbf/in;  $C_{AMD-24}=1.2$  lbf-s/in

## **2.5.2 Three-Disk Rotor**

### **2.5.2.1 Rotor with AMDs off**

The model of the three-disk rotor supported on its conventional bearings with the AMDs off for forced response is the same listed in Table 2.4 with the addition of an unbalance of 0.2 gr. placed at the midspan disk (station 7). This model was used as input file in the forced response code (MODLUND) of the Virginia Tech Rotordynamics Laboratory VT Fast program. The fluid film support bearing stiffness is approximated as 1800 lb/in, and the damping was approximated to 8 lb-s/in. Figure 2.40 shows the calculated forced response plot. For this configuration, the response amplitude expected at the first critical speed, 1600 RPM (26.7 Hz) is around 22.72 mils pp. A combination of high amplitudes due to vibration at the first critical speed and large shaft bow (which was not correctable) resulted in a rub of the shaft and the back-up bearing loosing the information as the rotor approached its first critical speed, as shown in the Bode plot of Figure 2.11. For this reason, the amplification factor of the experimental data could not be calculated. It is important to mention that the actual unbalance of the rotor is unknown and the value considered to perform the forced response analysis (0.2 gr) was estimated at first and was found to match the experimental data.

### **2.5.2.2 Rotor with the AMD-13 on**

A third bearing was added to the previous rotor model at station nine to account for the effect of turning the AMD-13 on. A stiffness of 1800 lbf/in and a damping of 8 lbf-s/in were used for the fluid film support bearings characteristics. The equivalent stiffness and damping associated with the AMD-13 were calculated, resulting in 1400 lbf/in and 2.95 lbf-s/in, respectively. These values were introduced in the forced response model but it was found that a stiffness of 600 lbf/in and a damping of 1.2 lbf/in produced a better match with the experimental results. Figure 2.41 shows the calculated forced response plot. For this configuration, the response amplitude expected at the first critical speed, 1950 RPM (32.5 Hz) is around 5.0 mils pp. The response amplitude expected at the second critical speed, 3500 RPM (58.3 Hz) is around 8.6 mils pp. The

calculated amplitudes agree with the amplitudes obtained experimentally, as shown in the Bode plot of Figure 2.36.

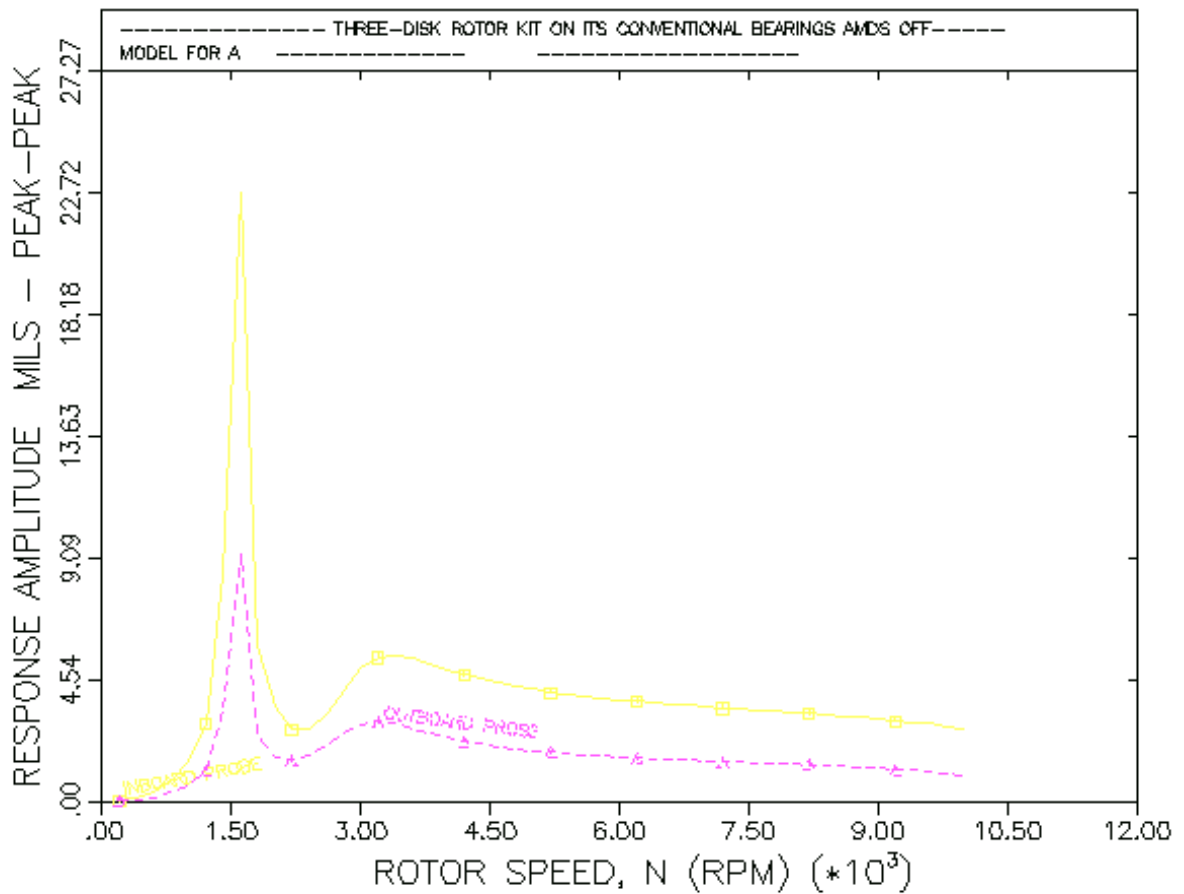


Figure 2.40: Forced response of the three-disk rotor supported on its conventional bearings with the AMDs off. Fluid film support bearing  $K=1800$  lbf/in;  $C=8$  lbf-s/in

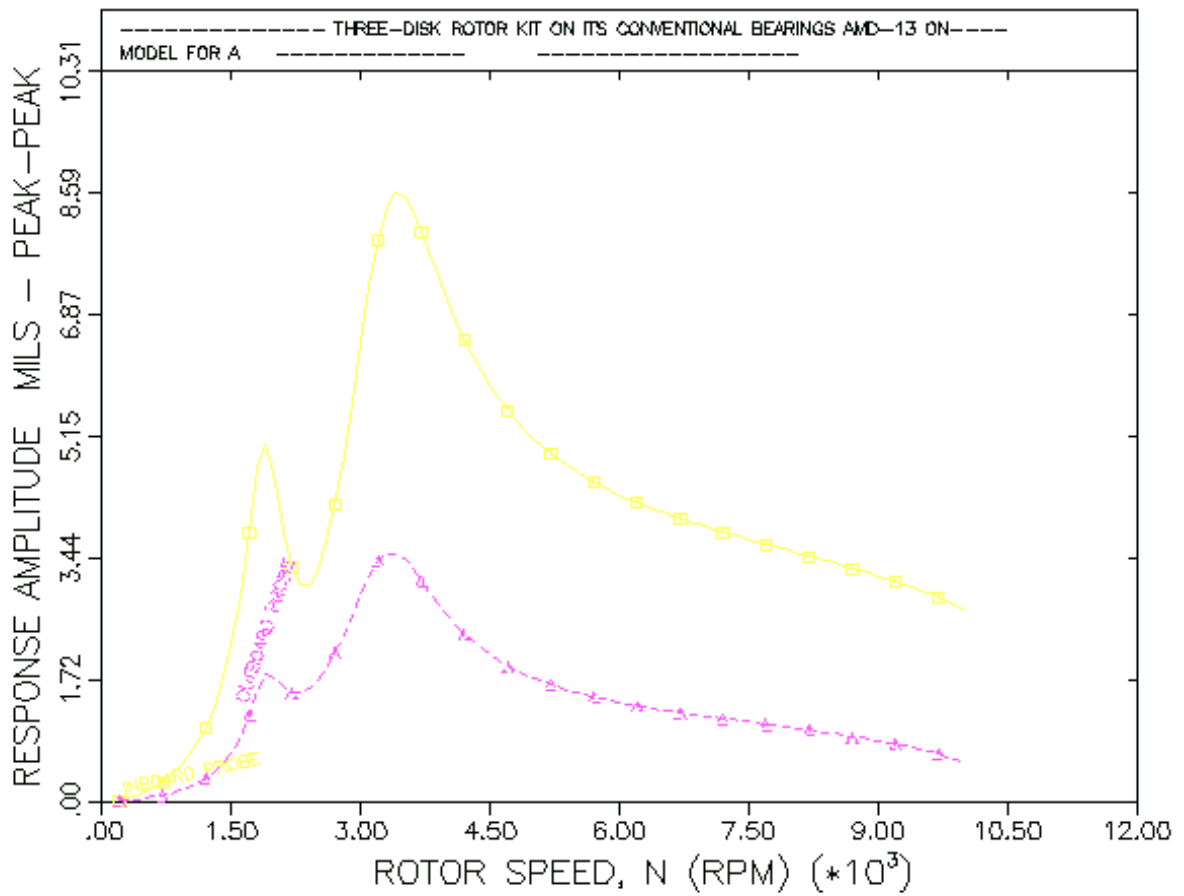


Figure 2.41: Forced response of the three-disk rotor supported on its conventional bearings and the AMD-13. Fluid film support bearings  $K=1800$  lbf/in;  $C=8$  lbf-s/in;  $K_{AMD-13}=600$  lbs/in;  $C_{AMD-13}=1.2$  lbf-s/in

### **2.5.2.3 Rotor with the AMD-24 on**

A third bearing was added to the previous rotor model at station five to account for the effect of turning the AMD-24 on. A stiffness of 1800 lbf/in and a damping of 8 lbf-s/in were used for the fluid film support bearings characteristics. The equivalent stiffness and damping associated with the AMD-24 were calculated, resulting in 1400 lbf/in and 2.95 lbf-s/in, respectively. These values were introduced in the forced response model but it was found that a stiffness of 800 lbf/in and a damping of 1.3 lbf/in produced a better match with the experimental results. Figure 2.42 shows the calculated forced response plot. For this configuration, the response amplitude expected at the first critical speed, 1900 RPM (31.7 Hz) is around 14 mils pp and the response amplitude expected at the second critical speed, 3850 RPM (64.2 Hz) is around 5.7 mils pp. The calculated amplitudes are close to the amplitudes obtained experimentally, as shown in the Bode plot of Figure 2.32.

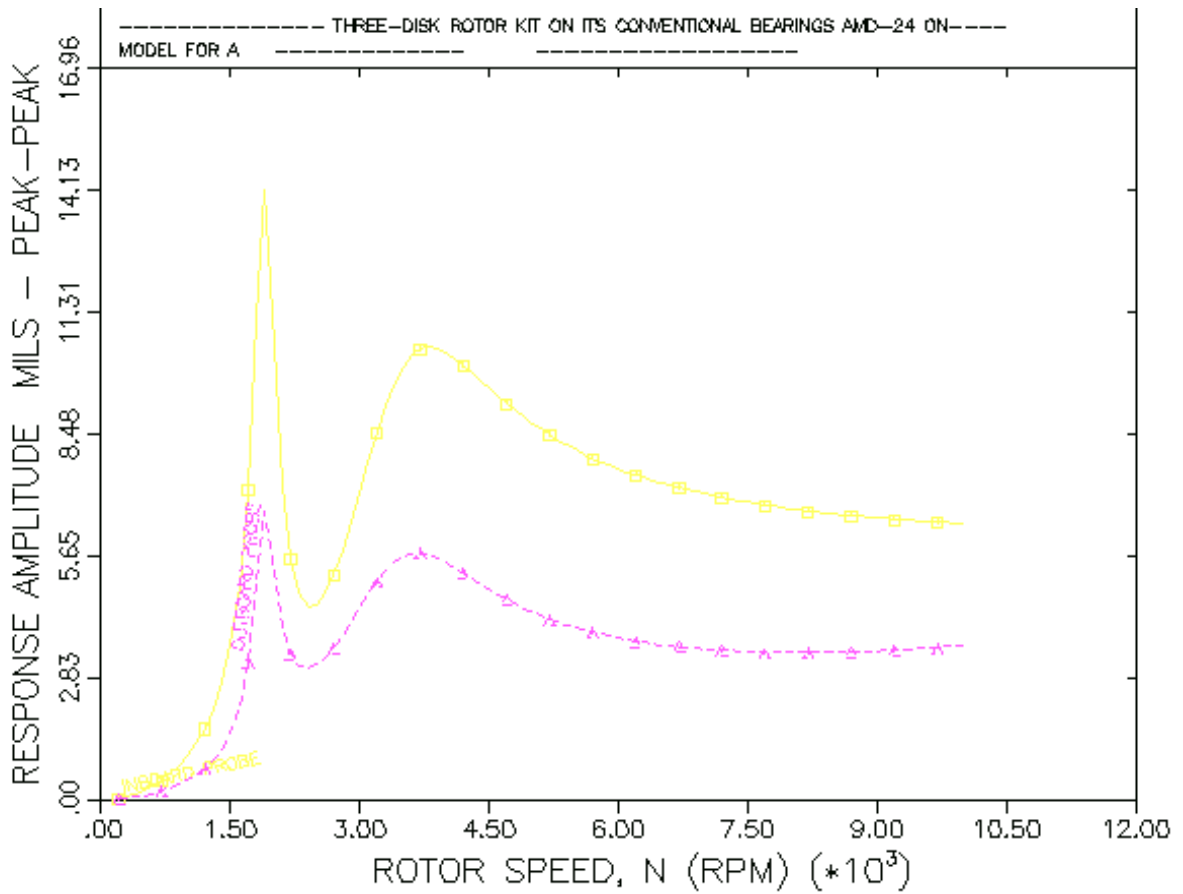


Figure 2.42: Forced response of the three-disk rotor supported on its conventional bearings and the AMD-24.  $K=1800$  lbf/in;  $C=8$  lbf-s/in;  $K_{AMD-24}=800$  lbf/in;  $C_{AMD-24}=1.3$  lbf-s/in